Thermodynamic modeling of hydrothermal ore deposit formation

Gleb S. Pokrovski

Journal Pre-proofs

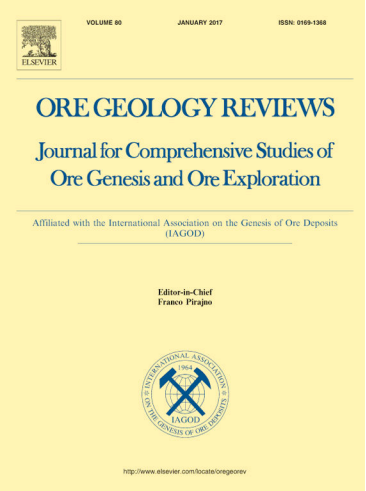

Thermodynamic modeling of hydrothermal ore deposit formation

Gleb S. Pokrovski

PII: S0169-1368(24)00569-9
DOI: https://doi.org/10.1016/j.oregeorev.2024.106436
Reference: OREGEO 106436

To appear in: *Ore Geology Reviews*

Received Date: 9 July 2024
Revised Date: 25 December 2024
Accepted Date: 25 December 2024

Please cite this article as: G.S. Pokrovski, Thermodynamic modeling of hydrothermal ore deposit formation, *Ore Geology Reviews* (2024), doi: https://doi.org/10.1016/j.oregeorev.2024.106436

Thermodynamic modeling of hydrothermal ore deposit formation

Gleb S. Pokrovski

Experimental Geosciences Team (GeoExp), Géosciences Environnement Toulouse (GET), UMR 5563 of the Centre National de la Recherche Scientifique (CNRS), Université Paul Sabatier Toulouse III, Institut de Recherche pour le Développement (IRD), Centre National d'Etudes Spatiales (CNES), Observatoire Midi-Pyrénées, 14 av. Edouard Belin, F-31400 Toulouse, France

e-mail: gleb.pokrovski@get.omp.eu; glebounet@gmail.com

Ore Geology Reviews

Revision 1

December 2024

Outline

Highlights

- Introducing thermodynamics of fluid-mineral interactions for beginners
- Describing the physical-chemical properties of geological fluids
- Overviewing aqueous speciation and thermodynamic models
- Highlighting case examples of numerical modeling for hydrothermal gold deposits
- Outlining perspectives and links with other approaches

Keywords

hydrothermal fluid, ore deposit, fluid-rock interactions, chemical speciation, mineral solubility, metal complexes, thermodynamic properties, gold; sulfur; carbon

Declaration of interests

☒ The authors declare that they have no known competing financial interests or personal relationships that could have appeared to influence the work reported in this paper.

☐ The authors declare the following financial interests/personal relationships which may be considered as potential competing interests:

Graphical Abstract

Click here to access/download;Graphical Abstract;GraphAbstract_OrGeo_submited.png

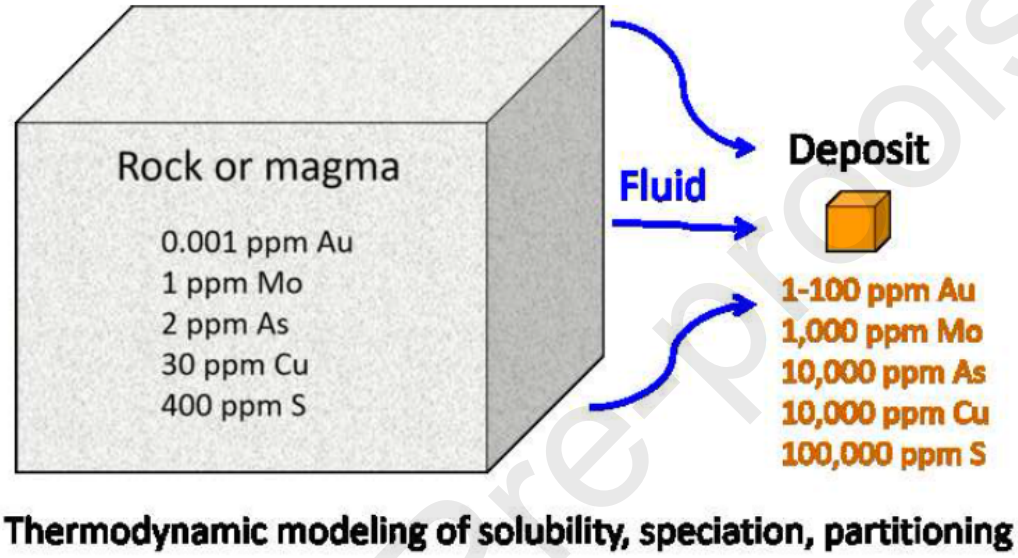

Abstract:

This contribution provides an introductory overview of the chemical thermodynamic modeling approach used in the field of hydrothermal mineral deposit research. An outline of our current knowledge of the physicochemical properties of geological fluids as a function of temperature, pressure, and density is presented. Currently, solubilities of major minerals and metal speciation can be predicted relatively accurately by thermodynamic calculations within the liquid-like density range of hydrothermal fluids. Metal-ligand chemical affinities and stabilities of aqueous complexes in such fluids are reviewed for main groups of metals. The fundamentals of the approach are first introduced in terms of chemical reactions of mineral solubility and dominant aqueous metal complexes. Using gold as an example, it is shown how this first-order approach can place valuable constraints on gold solubility and precipitation mechanisms, greatly aiding the interpretation of natural observations. The use of thermodynamic databases and computer codes for multicomponent systems is introduced, followed by a discussion of caveats and current limitations. Two more detailed examples of case studies of hydrothermal gold ore-forming systems, in porphyry and sedimentary contexts, highlight the value of complementary information that modeling can bring to naturalistic approaches. An overview of key challenges and emerging perspectives in fluid-rock interaction modeling concludes this article.

Graphical abstract:

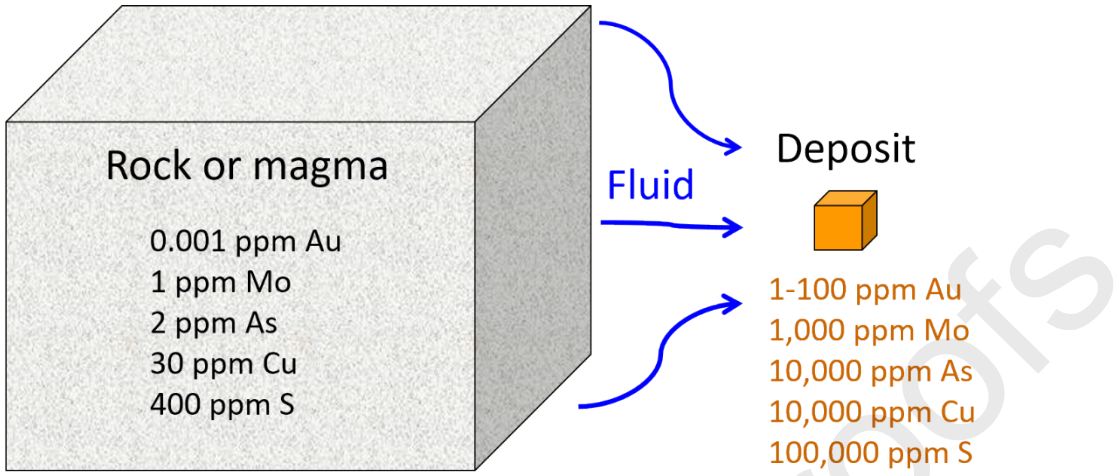

Thermodynamic modeling of solubility, speciation, partitioning

1. Introduction

On the global geochemical scale, mineral ore deposit formation on Earth is a very rare phenomenon. This is because the amount of a chemical element commodity in nowadays economically exploitable deposits is infinitely small compared to the total amount of this element the Earth's crust (e.g., 10,000 and 1,000,000 smaller for copper and gold, respectively). Ore-forming processes lead to metal concentration factors of thousands to a million relative to the average metal abundances in common crustal rocks. Such an exceptional phenomenon results from a favorable combination of a number of different factors. These span from the availability of a metal source and necessary amount of water to a heat source, from favorable geodynamics and tectonics to sufficient rock permeability allowing the fluid flow or circulation, and to efficient chemical and physical barriers triggering metal precipitation. These and other factors operate in combination, thereby allowing metal economic accumulation in the right place at the right moment within the Earth's crust, which would be impossible to imagine without a fluid phase. Therefore, the chemical speciation in the fluid phase and the solubility of both ore and gangue minerals at elevated temperatures and pressures is necessary for quantifying the processes and conditions that have led to the formation of an ore deposit and controlled its subsequent evolution. Although we, geologists, have sufficient access to ore – the ultimate product of such fluid-mineral(-melt) interactions at depth, the fluid phase itself remains very poorly accessible. While valuable direct evidence comes from fluid inclusions trapped in minerals during their growth or deformation, such data remain quite limited both due to intrinsic rarity and poor preservation of analyzable inclusions. Modern geothermal sources and volcanic gases also provide precious information of the fluid chemistry, but they generally probe near-surface conditions that may not fully reflect the amplitude of fluid-mineral reactions operating at depth.

Independent approaches are therefore required to better reconstruct the properties of the metalliferous fluid phase and its transformation reactions during ore deposit formation. One of them is thermodynamic modeling. It provides theoretical quantification of the concentrations and chemical speciation of metals and volatiles of the fluid phase and their changes upon fluid evolution in pressure-temperature-depth space during chemical reactions with rocks or other fluid reservoirs. The essential feature of this modeling is the assumption of chemical equilibrium, which allows us to use existing databases of thermodynamic properties for minerals, gases and dissolved species. Indeed, thermodynamic equilibrium is a plausible assumption for most reactions occurring within the fluid phase as well as for many reactions between an aqueous solution (or a gas) and solid phases at elevated temperatures relevant to ore deposit formation in hydrothermal and magmatic contexts. The main reason allowing us to assume equilibrium is because, in general, the rates of all chemical reactions greatly increase with increasing temperature, enabling a faster approach to equilibrium at temperatures well above ambient. However, some redox reactions, in particular those involving carbon (CH_4-C-CO_2), sulfur (H_2S-SO_4) or nitrogen (NH_3-N_2-NO_3), may yet be remarkably slow at moderate-temperature hydrothermal conditions (≤300 °C). In such cases, thermodynamics serves only as a guide of what would be expected if equilibrium were attained in the given system, thereby providing indications of the rates and duration of fluid-rock interactions. Needless to say that extreme care should be taken when applying equilibrium thermodynamic modeling to low-temperature near-surface environments. In fact, many chemical reactions appear to be "kinetically frozen" at such conditions (i.e. they are too slow to proceed within a reasonable timeframe of geological events). A funny example is the N_2-O_2-H_2O water-gas system at the

Earth's surface for which, if chemical equilibrium could be attained, we would have been swimming in concentrated nitric acid.

This overview is focused on chemical speciation and equilibrium in fluid-mineral systems in a hydrothermal-magmatic context where both elevated temperature and sufficiently long durations of ore deposit formation allow such systems to reasonably approach equilibrium, thereby enabling the application of chemical equilibrium thermodynamics. After a brief overview of our chemical and thermodynamic knowledge of geological fluids, key fundamentals of reaction thermodynamics applied to mineral-fluid systems are presented. Thermodynamic databases and associated computer tools allowing calculations in multicomponent systems are briefly introduced. The uncertainties and current limitations of this approach are highlighted. A concluding remark is offered regarding the remaining challenges and emerging perspectives of the thermodynamic modeling method, which is greatly enhanced through its integration with other complementary approaches.

This overview is intended for students, geoscientists, and economic geologists who have limited familiarity with the physical chemistry of aqueous solutions but are interested in applying thermodynamic modeling to enhance their understanding of ore-forming processes in a hydrothermal context. For these reasons, specific details and extensive comparisons are intentionally avoided in light of the vast body of experimental and thermodynamic data and models for aqueous species and minerals. The literature references are kept to a reasonable minimum to provide an inexperienced reader with a general overview without becoming overwhelmed by the intricacies of thermodynamic analysis.

2. Key physical-chemical properties of ore-forming fluids in the crust

2.1. Chemical composition of hydrothermal fluids

Fluids are essentially aqueous on Earth, accounting for 1–2% of the total Earth's crust rock volume. Therefore, in a first approximation, one might assume that a hydrothermal fluid moving through the largely dominating rock should closely match the rock elemental composition. Table 1 reports typical element concentrations of hydrothermal fluids compared to the corresponding Clarke values of the upper continental crust. The compositional data on hydrothermal fluids stem either from direct fluid sampling in active geothermal areas or from analyses of fluid inclusions that have been trapped by minerals (mostly quartz, but also topaz, calcite, fluorite, or sphalerite) during ore formation. It can be seen that the element concentrations in the fluids are both very different and much more variable compared to their corresponding crustal values. For example, major elements such as Si, Al or Fe are by many orders of magnitude depleted in the fluid phase compared to their average crustal abundance, whereas volatile elements, such as C, S, halogens, B or As, are typically strongly enriched in fluids versus common rocks. Alkali metals (Na and K), being almost in identical tenors in crustal rocks, show spectacular fractionations in the fluids with Na/K ratios up to 10 times greater than in the rock. The concentrations of base metals (Cu, Zn, Pb) in the fluid phase exhibit orders-of-magnitude variations. These observations clearly demonstrate that the fluid phase composition cannot simply be approximated by that of the rock with which the fluid interacts. These interactions are fundamentally controlled by specific fluid-mineral chemical reactions involving different molecular entities, called species or complexes, formed by chemical

elements in the fluid phase. Their molecular composition and thermodynamic stability are required to allow us to assess the role of fluids in geological processes. Our knowledge of these parameters is highly variable among the different fluid types and is strongly temperature- and pressure-dependent, as discussed in the following section.

2.2. State of knowledge of physical-chemistry of geological fluids and limits of applicability of thermodynamic modeling for the fluid phase

Geological fluids operate in a wide range of temperatures (from 0 to ~1000 °C) and depths (from Earth's surface to 100 km down), over which the physical-chemical properties of water and water-salt-gas systems and, consequently, their capacities to dissolve minerals and to transport chemical elements are markedly disparate. The principal types of geological fluids are illustrated in Figure 1 in the water phase diagram, showing the domains of the liquid, vapor, and supercritical fluid phases as a function of temperatures (*T*) and pressures (*P*) typical of the Earth's crust. Although there is a continuity between all fluid types in *T*-*P*-depth geological space, our physical-chemical knowledge of the fluids is not continuous, and the available experimental and theoretical approaches used for their study are not uniform. Understanding the impact of these different fluid types on geological processes requires knowledge of the solubility of minerals and the speciation and partitioning of chemical elements in the different fluid and mineral phases. Our ability to numerically predict these parameters significantly varies across the *T*-*P* range, as illustrated by the three fields identified in Fig. 1. In the domain of aqueous solutions at moderate temperatures (blue, labeled A), a large amount of data exists on the identity and stability of the major metal complexes. Thermodynamic models based on these data have been developed over >50 years for predicting ore mineral solubilities and fluid-rock interactions (e.g., Brimhall and Crerar, 1987; Helgeson et al., 1981; Barnes, 1997; Wood and Samson, 1998; Oelkers et al., 2009; Stefansson et al., 2013 to name a few). In contrast, it is only in the last 10-20 years that new insights have been gained into the speciation and transport of economic metals in low-density vapor phases typical of hydrothermal-magmatic deposits (pink area, labeled B in Fig. 1). Nevertheless, our ability to numerically predict vapor-phase metal transfers is still rather limited (see Liebscher and Heinrich, 2007; Pokrovski et al., 2013a for a review). Similarly, our current knowledge is still insufficient in the domain of high-pressure fluids typical of subduction zones (gray area, labeled C in Fig. 1). In this domain, large uncertainties persist as to the quantitative estimation of the effect of the major ligands like chloride, sulfur, carbon or silica on metal mobility (e.g., Manning, 2018). Recent extensions of the thermodynamic models of the fluid phase (HKF, density model, see below) based on experimental data enable nowadays reasonable predictions of solubility above 5 kbar for a limited number of elements and minerals.

Because the density of the aqueous phase varies over several orders of magnitude across the *T*-*P* range of terrestrial processes, it is convenient to consider the different types of aqueous fluid phases in terms of density. Indeed, the capacity of these fluid phases to carry and fractionate chemical elements is primarily a function of temperature and fluid density. In this chapter, I will use the term "fluid" for an aqueous, commonly salt-bearing, solution whose density is greater than the water critical density (>0.3–0.4 g/cm^3). This term implicitly includes the "liquid phase" domain whose upper limit is commonly defined by the critical point of water (374 °C and 221 bar). The term "vapor" is used here to refer to a volatile fluid phase produced by magma degassing and/or fluid boiling over a wide *T* range (100–1000°C) and whose density is less than the critical density of the given fluid composition. The vapor domain may in turn be divided into two sub-types, which mostly differ from one another by their density: volcanic

vapors and hydrothermal-magmatic vapors (Fig. 1). Typical density ranges at magmatic-hydrothermal(-metamorphic) conditions on Earth are <0.001–0.4 g/cm^3 and 0.4–1.0 g/cm^3 for vapor and liquid phases, respectively.

In this article, the focus will be on the liquid-like fluids delimited by domain (A), for which more extensive and robust thermodynamic information is currently available than for domains (B) and (C). Thermodynamic modeling of fluid-mineral reactions requires two key things: first, knowledge of the chemical speciation of the dissolved elements in the fluid phase, and second, numerical values for reaction constants. These requirements are discussed in the following sections.

2.3. Chemical speciation of elements in the fluid phase

Chemical elements are dissolved in aqueous solution in the form of cations (positively charged ions formed by most metals, e.g., Ag^+, Fe^{2+}, Zn^{2+}, Al^{3+}) and anions (negatively charged ions formed by non-metals, usually called ligands, e.g., Cl^-, SO_4^{2-}, HS^-). The ions are all hydrated to varying degrees by water molecules, which can be seen "directly" by some spectroscopic methods (e.g., X-ray absorption or nuclear magnetic resonance spectroscopy). For example, the Ag^+ cation is surrounded by four water molecules in its first-shell coordination sphere, forming the $Ag(H_2O)_4^+$ entity, with additional weakly bound H_2O molecules in the outer-sphere, while the Cl^- anion is more loosely solvated by H_2O with a less clearly defined coordination sphere. Both types of ions can associate with each other, usually by displacing a water molecule from the Ag first coordination sphere and forming a direct chemical bond (Ag–Cl)

$$Ag(H_2O)_4^+ + Cl^- = AgCl(H_2O)_3^0 + H_2O \quad (1a)$$

Given that the water activity is approximately one in an aqueous fluid phase, this reaction may be simplified for thermodynamic modeling purposes by omitting the water molecules

$$Ag^+ + Cl^- = AgCl^0 \quad (1b)$$

Here, all reaction components are aqueous species, which should not be confused with gaseous ions, which have different thermodynamic properties and reference states (see section 4 for definition).

With increasing salt content in the fluid and raising temperature, such associates become more abundant and more ligands may are bound to the cation (e.g., forming $AgCl_2^-$ and higher order chloride complexes, $AgCl_3^{2-}$ and $AgCl_4^{3-}$). All cations, anions and their complexes are present simultaneously in the aqueous fluid phase, but at different concentrations (or activities). This property contrasts to a pure mineral phase (e.g., pyrite, sphalerite or hematite) whose thermodynamic activity is either 1 or 0 and whose formation and disappearance in *T*-*P*-composition space is governed by the phase rule. The notion of activity makes the fundamental physical-chemical difference between a pure phase and an aqueous species often misunderstood by geologists. The total metal content in the fluid phase is always the sum of all species concentrations:

$$\Sigma Ag_{(aq)} = Ag^+ + AgCl^0 + AgCl_2^- + AgCl_3^{2-} + AgCl_4^{3-} \quad (1c)$$

Other non-chloride species may be added to this total (e.g., hydrosulfides). However, among the multitude of aqueous species for a given metal, all present simultaneously in the fluid phase, there is usually one or a few that are dominant (i.e., most concentrated) at given *T-P* conditions and fluid composition, while all other species are often much less abundant. For example, in the case of Ag, $AgCl_2^-$ is the dominant complexes in most saline hydrothermal fluids at temperatures above 200–300 °C while $AgCl^0$ as well as $AgCl_3^{2-}$ and $AgCl_4^{3-}$ are much less abundant and the Ag^+ cation itself is virtually negligible (e.g., Pokrovski et al., 2013b). As a result, the latter four species can be safely neglected because their contribution to the total amount of metal transported by the fluid would be very small.

What are the dominant complexes for a given metal in hydrothermal fluids? For example, why are they chlorides for zinc or silver, but sulfides and polysulfides for gold and platinum? Their nature is determined by two factors: i) the chemical affinity of the metallic element for a particular ligand, and ii) the abundance of the ligand itself in the fluid. Metal-ligand affinities are fundamentally defined by the electronic structure of the complexing elements. These affinities may be predicted using the so called soft-hard classification of chemical elements (hard and soft acid and base theory, HSAB) appeared in chemistry in the 1960s (Pearson et al., 1963; Pearson, 1997 and references therein). While behind this theory are numerical functions such as ionization potential, bond-dissociation energy and electronegativity, the concept itself is simple and elegant. It is outlined below for a general reader who is also referred to Crerar et al. (1985), Brimhall and Crerar (1987), Wood and Samson (1988), and Barnes (1997) for more details and variations of presentation. According to this concept illustrated in Fig. 2, metal cations (called acids) may be divided into three categories. The first, shown in red, contains either small and strongly charged (Be^{2+}, B^{3+}, Zr^{4+}, Nb^{5+}) or big and easily ionizable (Cs^+, Ba^{2+}) cations. They are termed “hard” because their electronic clouds are hard to deform (or polarize) to be able to share electrons with ligands in a chemical bond. These types of chemical bonds are called ionic and are provided by dominant electrostatic attractions between the charged cation and anion spheres. The second category, shown in blue, contains large, weakly charged and easily polarizable cations (e.g., Ag^+, Au^+, Pt^{2+}), with electronic clouds that can be easily deformed to allow sharing of electrons with a ligand in a chemical bond. Such bonds are called covalent bonds. The third (intermediate or often called borderline) category of metals is shown in yellow. Analogous three types also apply to non-metals (or ligands, also called bases), with O^{2-}, OH^-, F^- and C^{4+} (as carbonate CO_3^{2-}) being hard, Br^-, I^-, Te^{2-} – soft, and Cl^- – intermediate.

The basic rule is that a soft "loves" a soft and a hard "loves" a hard, i.e. hard metal cations prefer to complex with hard ligands and soft metals with soft ligands. The degree of hardness (or softness) also depends on the oxidation state of the element, with higher oxidation states being harder. Sulfur is an excellent example of such a dualism as it forms both very soft sulfide (S^{2-}) and very hard sulfate (S^{6+}). Similarly, arsenic and antimony in their highest oxidation state of +5 as arsenates and antimonates (shown in the red upper right corner of their respective cells in Fig. 2) form almost exclusively oxyhydroxides both in aqueous solution and in the solid phase at the Earth’s surface. The most reduced formal states of –1 to –3 as arsenides and antimonides (shown in blue in the lower left corner of their cells in Fig. 2) make these elements soft ligands similar to sulfide. Finally, in their intermediate oxidation state of +3 (not shown), both oxyhydroxide (hard) and sulfide (soft) complexes and minerals occur for As and Sb in reduced sedimentary environments and geothermal systems. Although qualitative, this classification not only elegantly explains the prevalence of the various complexes in aqueous solution, but also reflects the general distribution of elements on Earth, since it is also applicable to solid phases. Remarkably, the hard-soft classification strongly resembles the geochemical classification of elements as lithophile (i.e. SiO_2-loving and therefore hard), chalcophile (i.e.

copper-loving meaning reduced sulfur-loving such as in the main copper ore chalcopyrite, $CuFeS_2$, and therefore soft), and siderophile (iron-loving and, therefore, intermediate). Thus, a hard metal cation, such as La^{3+} representative of the group of rare earth elements (REE), forms the most stable complexes with the hardest ligand of the halogen group, F^-, while a moderately soft cation, Ag^+, forms the strongest complexes with I^-.

However, this does not mean that fluoride and iodide complexes, respectively, would be the dominant types transporting REE and Ag by most hydrothermal fluids. Another parameter – the ligand concentration itself – must be taken into account. In fact, fluorine is a minor component of most hydrothermal fluids (Table 1) because of the poor solubility of its solid phases, such as fluorite and apatite, and its much stronger affinity for silicate minerals and melts than for aqueous fluids. Similarly, iodine concentrations in the fluids are usually negligible due to its very low natural abundance (average I concentration in the upper continental crust is only ~0.1 ppm; Rudnick and Gao, 2014). Consequently, neither F^- nor I^- ligands are present in sufficient concentrations to complex La and Ag. As a result, for both metals and their respective analogs, chloride complexes are largely dominant due to the simple fact that Cl^- is by far the most abundant ligand in various types of hydrothermal fluids.

Our current knowledge of the main complexes of different elements in typical hydrothermal fluids is resumed in Table 2. The data presented are the result of a large number of experimental (mostly solubility), in situ spectroscopic as well as theoretical studies, mostly since the 1950s. This work has established the stoichiometry of the dominant metal complexes and generated their stability constants over the hydrothermal *T-P* range of aqueous liquid-like fluids (blue area (A) in Fig. 1). For details on methods, complexation peculiarities, mechanisms and coordination changes depending on the element, the reader is referred to the representative publications listed in Table 2 as well as to detailed reviews and compilations (Baes and Mesmer, 1976; Brimhall and Crerar, 1987; Jolivet et al., 1994; Martell and Hancock, 1996; Barnes, 1997; Wood and Samson, 1998; Kouzmanov and Pokrovski, 2012; Pokrovski et al., 2014, 2025; Brugger et al., 2016; Migdisov et al., 2016).

Studies of chemical speciation in aqueous fluids at elevated temperatures and pressures, benefiting from state-of-the-art approaches, appear regularly in the chemical and geochemical literature (see also section 6). Our vision of the behavior of some elements is evolving and becoming "sharper" with the continued development of experimental, analytical, spectroscopic, and modeling approaches. Gold is a good example, for which at least 20 different sulfide, chloride and hydroxide complexes have been proposed in hydrothermal fluids over >80 years of research, of which only 3 have direct spectroscopic evidence along with robust and consistent thermodynamic data sets (see compilations of Pokrovski et al., 2014, 2025). The current situation for different groups of metals is the following. In typical hydrothermal fluids, most metalloids (As, Sb, Si) dominantly form uncharged hydroxide complexes. The speciation of transition and base metals (Fe, Cu, Ag, Zn, Pb) is largely dominated by chloride species. “Hard” metals (Al, Zr, Nb, Ti, Cr) mostly form hydroxide complexes. For rare earth elements (REE), chlorides and sulfates are likely to be most important while hydroxide and fluoride are generally subordinate. “Soft” metals (Au, Pd, Pt) largely prefer hydrosulfide (HS^-) ligands, while their chloride complexes may only be sufficiently abundant in highly acidic, saline and oxidized high-temperature fluids. An additional strong ligand for these metals, the trisulfur radical ion ($S_3^{\bullet-}$), has recently been discovered in hydrothermal-magmatic fluids in which sulfate and sulfide coexist (Pokrovski and Dubrovinsky, 2011; Pokrovski and Dubessy, 2015; Colin et al., 2020; He et al., 2025). In addition to the exact stoichiometry of the complexes reported in Table 2, our ability to predict metal solubilities also depends on the robustness of the stability constants for all these complexes. This parameter may be expressed in terms of the uncertainty

associated with thermodynamic calculations of ore and gangue mineral solubilities within the typical *T-P* domain of hydrothermal fluids (<600 °C, <2 kbar). The solubility of the major solid phases of metals and metalloids, such as As, Au, Ag, Si, Al, Cu, Zn, and Pb, in hydrothermal fluids may reasonably be predicted within 0.5–1 log units. The equilibrium predictions are much less precise for REE, which form different types of complexes depending on the fluid composition, and even more importantly, a variety of silicate, oxide and fluoride solid phases and solid solutions whose thermodynamic properties are poorly known, bringing additional uncertainty on the true solubility-controlling phase. Modeling trace elements that do not usually form their pure mineral phases but rather get incorporated into major-element sulfide, oxide or silicate minerals in chemically bound states (e.g., invisible gold in pyrite and arsenopyrite; see sections 4.1 and 6), is virtually non-existent because of the lack of a robust thermodynamic framework for such substitutions. This is also the case of Ga, Ge or Cd with relatively well known aqueous speciation (Table 2). Among the metals shown in Table 5, the "worst" situation is probably for Mo, and its "little brother" (Re, not shown) whose complexes with major ligands (such as Cl and S) are still very poorly known. The uncertainty of thermodynamic predictions generally grows with increasing *T* and *P*. Note that a typical error of one decimal log unit, inherent to the solubility of known metal complexes, can be considered a good precision given the much larger variability of natural metal concentrations, which typically exhibit variations of many orders of magnitude as analyzed in natural fluid inclusions (e.g., Yardley, 2005; Kouzmanov and Pokrovski, 2012).

3. Fluid-mineral interactions in terms of dominant chemical reactions

Once we know for a given metal its dominant species and its stability constant in the fluid phase, in many cases the solubility of the metal-bearing ore mineral can be quantitatively evaluated by analyzing elementary chemical reactions, without the need for sophisticated computer codes. Such an approach should be considered as the first step in interpreting fluid-rock interactions. For example, in the case of gold in the majority of epithermal sulfur-bearing fluids, the gold dissolution (or precipitation) controlling reaction is the following:

$$Au(HS)_2^- + 0.5\ H_{2(aq)} + H^+ = Au_{(s)} + 2\ H_2S_{(aq)} \qquad (2a)$$

where (s) denotes the Au-bearing solid phase (native metal), and all other reaction constituents are aqueous species (aq) in the fluid phase. The equilibrium constant of this reaction, according to the mass action law, is written as

$$K_{T,P} = \frac{a(H_2S)^2}{a(Au(HS)_2^-) \times a(H_2)^{0.5} \times a(H^+)} \qquad (2b)$$

where *a* is the thermodynamic activity of each indicated species equivalent to its concentration (see section 4 for rigorous thermodynamic definitions). Note that $Au_{(s)}$ metal is omitted is this equation because it is a pure phase whose activity is equal to one by definition. The fundamental property of a thermodynamic equilibrium constant is that its value at given *T* and *P* is independent of the system chemical composition. Therefore, identifying the dominant reaction, along with knowledge of its thermodynamic constant value, allows direct quantification of Au solubility as a function of the fluid H_2S and H_2 concentrations and acidity (pH). These three

parameters may either be directly obtained from sampled geothermal fluids (e.g., Hannington et al., 2016; Simmons et al., 2016) or accessed in ancient deposits from fluid-inclusion analyses (e.g., Kouzmanov and Pokrovski, 2012) and major mineral assemblages that act as redox or pH buffers. For example, the hematite-magnetite assemblage, common in porphyry systems, defines the value of oxygen fugacity, f_{O_2}, and consequently of f_{H_2}, via the following equilibria

$$Fe_3O_{4\ (magnetite)} + 0.25\ O_{2(g)} = 1.5\ Fe_2O_{3\ (hematite)} \quad (3)$$

$$H_{2(g)} + 0.5\ O_{2(g)} = H_2O_{(l)} \quad (4),$$

where $\log f_{O_2} = -4\times\log K_3$, and $\log f_{H_2} = -\log K_4 - 0.5\times\log f_{O_2}$. Similarly, the alkali-aluminosilicate assemblage of quartz, potassic feldspar and muscovite, common for felsic rocks hosting porphyry deposits, buffers the pH in equilibrium with a KCl-bearing fluid

$$1.5\ KAlSi_3O_{8\ (K\text{-}feldspar)} + H^+ = 0.5\ KAl_3Si_3O_{10}(OH)_{2\ (muscovite)} + 3\ SiO_{2\ (quartz)} + K^+ \quad (5),$$

where the ratio $a(K^+)/a(H^+) = \log K_5$ at given *T-P* and is independent of the fluid composition.

Table 3 reports typical values of aqueous H_2S and H_2 concentrations and pH determined in modern geothermal fluids and porphyry-epithermal Cu-Au-Mo deposits, of an average salinity of 6 wt % NaCl equivalent. The resulting Au solubility in such a fluid can thus be calculated directly from equation (2b) using the reaction K_2 values reported in the literature (e.g., Pokrovski et al., 2014), and the activities of H_2 and H_2S approximated by their respective concentration values. Note that such calculations must be made on the molality scale for aqueous species concentrations (i.e. number of moles of the species per 1 kg of water, m) because, by convention, all thermodynamic constants are related to this concentration scale (see section 4). It can be seen in Table 3 that the calculated Au solubility values are well within the range of natural Au concentrations reported for medium temperature (~300 °C) geothermal and epithermal fluids. This agreement strongly supports both the validity of the thermodynamic constant values for $Au(HS)_2^-$ and the robustness of the elementary reaction approach for well-constrained fluid compositions.

In contrast, calculations for higher *T-P* porphyry fluids underestimate, up to 200 times, Au concentrations as compared to direct analyses of fluid inclusions from such settings. This discrepancy, in general, may be due to three potential issues, acting alone or in combination: i) poor knowledge of the reaction (2) constant value at such high *T-P* conditions due to lack of experimental data or imperfections of the thermodynamic models used for its estimation; ii) poor assessment of the H_2S, redox and pH values in the natural fluid; and iii) the predominance, at these *T-P* conditions, of Au-bearing species other than $Au(HS)_2^-$. The quantitative assessment of these issues, inherent in any thermodynamic modeling of fluid-rock interactions, should be made on a case-by-case basis, as it is highly dependent on both the metal/reaction itself (see Table 2) and the detailed geochemical context. For the present example of Au, it seems very likely that reasons (i) and (ii) are subordinate, and reason (iii) is most important. Indeed, novel stable Au-bearing complexes formed with the $S_3^{\bullet-}$ ion, such as $Au(HS)S_3^-$, have recently been identified at such conditions (Pokrovski et al., 2015, 2022a, see section 5). They should therefore be taken into account in the solubility calculations, in addition to reaction (2). More generally, the modeler should be aware of the uncertainties intrinsic to the three issues above, combined with the large magnitude of fluid composition variations in nature. For example, a change of one order of magnitude in the H_2S concentration alone would result in a corresponding change of two orders of magnitude in the Au concentration, according to the stoichiometry of reaction (2a). This is simply because a change in the concentration of one of

the reaction components at equilibrium must be compensated for by an increase or decrease in the $Au(HS)_2^-$ concentration to keep the K_2 value constant (equation 2b).

As a result, equations (2a) and (2b) offer a straightforward assessment of the effect of key fluid parameters on gold precipitation. Thus, a decrease in H_2S concentrations (e.g., via fluid boiling, interactions with FeO-bearing rocks, and/or oxidation by meteoric waters) would favor Au precipitation, if the other parameters (i.e. redox, acidity) remain unchanged. Fluid reduction (e.g., via interactions with organic carbon-bearing rocks) would increase H_2 concentrations and shift reaction (2a) to the right, thereby leading to gold precipitation. Fluid acidification (e.g., through hydrolysis of magmatic SO_2 to H_2S and sulfuric acid – a process common in porphyry systems, e.g., Fontboté et al., 2017) would also favor gold precipitation for the same reason. However, in many natural situations, a change of one parameter is accompanied by concomitant changes of the other parameters. For example, boiling, which results in H_2S loss from the liquid phase and favors gold precipitation, is often accompanied by a decrease in H_2 and an increase in pH, both of which favor gold dissolution. The resulting effect on gold solubility is thus a fine interplay of all these parameters. Its quantitative evaluation would require more advanced numerical modeling in multi-component systems than is provided by the elementary reaction analysis above. The following section outlines the basics of such modeling.

4. Thermodynamic modeling in multicomponent fluid-mineral systems

4.1. Fundamental thermodynamic relationships and functions

Thermodynamic equilibrium calculations in most systems of geological interest require either the standard molar Gibbs energies for individual aqueous species, minerals or gases or, alternatively, equilibrium reaction constants. The equations and associated coefficients that describe these two fundamental variables as a function of T and P are stored in databases and evaluated by computer codes that will be reviewed in section 4.2. Here we define and briefly discuss fundamental thermodynamic relationships and equations for their practical use in modeling studies.

The Gibbs energy of individual aqueous or gaseous species or solid phase is defined as

$$G_{i,T,P} = \Delta G^0_{i,T,P} + RT \ln a_i \quad \text{(for solid and aqueous species)} \qquad (6)$$

$$G_{i,T,P} = \Delta G^0_{i,T,\mathrm{P}_r} + RT \ln f_i \quad \text{(for gases)} \qquad (7)$$

where $\Delta G^0_{i,T,P}$ = standard molar Gibbs energy of i-*th* species, a_i = activity (for aqueous or solid species), f_i = fugacity (for gaseous species), and ln is natural logarithm (≈2.3026 $\log_{10}$). The standard states commonly adopted in geochemistry of fluid-rock-gas interactions are the following (e.g., Oelkers et al., 2009): for solid phases – pure substance ($a_i = 1$); for gases – pure gas substance at 1 bar pressure and having an ideal-gas behavior ($f_i = P_i \times \varphi_i$, with fugacity coefficient $\varphi_i = 1$); for aqueous species – 1 molal (i.e. 1 mole per kg of H_2O) solution whose behavior is ideal ($a_i = m_i \times \gamma_i$, with activity coefficient $\gamma_i = 1$). For solid solutions, the

activity/concentration units of solid-phase species or mineral end-members are conventionally expressed as mole fraction ($a_i = x_i \times \gamma_i$). Note also that, by convention, all thermodynamic properties of the proton (H^+) in aqueous solution are equal to 0 at all T and P.

For the majority of geochemical purposes, the Debye-Hückel (DH) electrostatic model for activity coefficients of electrically charged aqueous species is commonly used (e.g., Helgeson et al., 1981):

$$\log_{10}\gamma_i = -A\, z_i^2 \sqrt{I}/(1+B\, \mathring{a}_i \sqrt{I}) + b\, I + \Gamma_\gamma \quad (8)$$

where A and B are the DH electrostatic parameters; I is the effective molal ionic strength ($I = 0.5 \sum z_i^2 m_i$); z_i and $\mathring{a}_i$ are, respectively, the ionic charge and the distance of the closest approach between ions; b is the extended DH parameter for electrolyte solutions depending of the dominant salt (e.g., NaCl, KCl); Γ_γ is the mole fraction to molality conversion factor, $\Gamma_\gamma = \log_{10}(1+0.018m^*)$, where m* is the sum of the molalities of all solute species. Note that the validity of this equation extends to very high salinities at elevated temperature (e.g., up to as much as 18 m NaCl at T>300 °C; Zotov et al., 2018). For uncharged aqueous species, equation (8) simplifies to

$$\log_{10}\gamma_i = \Gamma_\gamma + b_i\, I \quad (9)$$

where b_i is the empirical Setchenov coefficient, which is usually set at zero for neutral species thereby yielding activity coefficients close to one. Other more elaborate, but limited in T-P range and element selection, activity coefficient models, such as the Pitzer model, are also used to model mostly low-temperature brine-mineral interactions, typically in the context of evaporite reservoirs and geologic CO_2 storage in salt rock formations. Many computer codes offer a choice of activity coefficient models. Note, however, that in most applications to high-temperature (≥ 300 °C) hydrothermal-magmatic contexts, the exact choice of activity coefficient model has a relatively small impact compared to the uncertainties in the stability constants (or standard Gibbs energy) for most aqueous species. (see Table 2).

The change of standard Gibbs energy of a reaction is related to the reaction equilibrium constant as

$$\Delta_r G^0_{T,P} = \sum_i n_i \times G^0_{i,T,P} = -2.3026 RT \times \log_{10} K_{T,P} \quad (10)$$

where R is the ideal gas constant = 8.314 J/(mol K), T = temperature in Kelvin = T °C + 273.15, n_i is the stoichiometric coefficient of each reaction constituent, and $K_{T,P}$ is the equilibrium constant at given T and P of the generic reaction

$$wW + xX = yY + zZ \quad (11)$$

$$K = \frac{Y^y \times Z^z}{W^w \times X^x} \quad (12)$$

where W, X and Y, Z are activities of the reactants and the products, respectively, and w, x, and y, z are their respective stoichiometric coefficients in the reaction. Note that both $\Delta_r G^0$ and K depend on T and P, but do not depend of the system composition at given T and P. At equilibrium, the total Gibbs energy of the system is minimal

$$\Sigma G_{i,T,P} \rightarrow min \tag{13}$$

Depending on the computer program, thermodynamic equilibrium calculation algorithms either seek to minimize the total Gibbs energy of the system (equations 6 and 7) or solve the system of reaction equations (equations 11 and 12), in both cases by finding an appropriate set of species activities at equilibrium. Both algorithms apply mass and electrical charge balance constraints (i.e. the masses of the chemical elements in the system are conserved and the aqueous solution has an electrical charge of zero).

The major caveat of such calculations, often disregarded by many users of geochemical computer codes, is the reliability of estimations of numerical K and G^0 values at elevated T-P. The variation of the standard Gibbs energy with T and P of any phase or species may be obtained by integrating the heat capacity and volume functions over the T-P interval:

$$\Delta G^0_{i,T,P} = \Delta_f G^0_{i,T_r,P_r} - (T - T_r) \times S^0_{i,Tr,\mathrm{Pr}} + \int_{Tr}^{T} Cp_i^0 \, dT - T \int_{Tr}^{T} (Cp_i^0 / T) \, dT + \int_{\mathrm{Pr}}^{P} V_i^0 \, dP \tag{14}$$

where $\Delta_f G^0_{i,T_r,P_r}$ = molar Gibbs energy of formation from the elements at the reference temperature and pressure T_r and P_r, which are 25°C (298.15 K) and 1 bar (=0.1 MPa), respectively; S^0_{i,T_r,P_r} = molar entropy of the i-th species at T_r and P_r, and Cp_i^0 and V_i^0 = respectively, molar isobaric heat capacity and volume of the i-th species. It follows from equation (14) that knowledge of Cp_i^0 and V_i^0 as a function of T and P is required for accurate calculations of the ΔG^0 values (or equilibrium constants). Note that another thermodynamic function, the standard enthalpy, $\Delta_f H^0_{i,T_r,P_r}$, is a redundant variable in such calculations because it is directly related to Gibbs energy and entropy as

$$\Delta_f G^0_{i,T_r,P_r} = \Delta_f H^0_{i,T_r,P_r} - T \times \Delta_r S^0_{T_r,P_r} \tag{15}$$

where $\Delta_r S^0_{T_r,P_r}$ is the standard entropy change of the reaction of formation of the i-th species from elements in their stable states. As an example, the thermodynamic Gibbs energy and enthalpy functions of formation for the $Au(HS)_2^-$ aqueous complex are defined by the formal reaction:

$$Au_{(s)} + 1.5\ H_{2(g)} + 2\ S_{(s,l)} = Au(HS)_2^- + H^+ \tag{16}$$

where the elements gold, hydrogen and sulfur are in their standard stable states, i.e. their $\Delta_f G^0_{i,T_r,P_r}$ and $\Delta_f H^0_{i,T_r,P_r}$ values are zero.

The thermodynamic models for aqueous species, gases and solid phases at elevated T-P mostly differ in the way they treat the Cp^0 and V^0 functions. As a result, in most thermodynamic databases, the user will commonly find numerical values for the following thermodynamic parameters: ΔG^0 (and/or ΔH^0), S^0, Cp^0 and V^0 at 25 °C and 1 bar and sets of numerical T-P independent coefficients that describe the change of Cp^0 and V^0 values with temperature and pressure (e.g., SUPCRT92 or SUPCRTBL databases). Alternatively, some databases store $\log_{10}K$ (or $\ln K$) values of different reactions that cover the whole set of species and minerals in the system as a function of temperature using a set of empirical regression coefficients (e.g., PHREEQC or LLNL databases):

$$\log_{10}K = A_1 + A_2 \times T + A_3/T + A_4 \times \log_{10}T + A_5/T^2 \quad (17)$$

For most modeling applications in the hydrothermal(-magmatic/metamorphic) *T*-*P* space of shallow-to-middle crustal metal ore formation, the thermodynamic properties of pure minerals and gases are much better constrained than those of aqueous species. For example, ideal gas properties can reasonably approximate most gas-phase components up to pressures of several kbar. Similarly, the mineral expansivity and compressibility (described by the volume functions vs. *T* and *P*, e.g., in the SUPCRTBL or Perple_X database, see below) can be neglected to at least 10 kbar without introducing significant errors since their contribution to the Gibbs energy is rather small and moreover is (partially) compensated by the simultaneous increase in *T* and *P*. Major data sources and models of thermodynamic properties of solid phases and gases can be found in seminal compilations of Naumov et al. (1974), Wagman et al. (1982), Robie and Hemingway (1995), Chase et al. (1998) and Holland and Powell (2011).

Models for aqueous species are more sophisticated and more challenging. The most widely used model to describe the thermodynamic properties of aqueous species at hydrothermal conditions is the HKF model (named in honor to its developers – Helgeson, Kirkham, Flowers; Helgeson et al., 1981), largely revised and extended in subsequent papers of Helgeson's group (e.g., Sverjensky et al., 1997, 2014) and incorporated in thermodynamic databases, such as SUPCRT92 (Johnson et al., 1992) and SUPCRTBL (Zimmer et al., 2016). This model applies to the majority of metal aqueous species cited in Table 2. Other, less commonly used, models to describe thermodynamic properties of aqueous species or reaction constants at elevated *T*-*P* include the density model (e.g., Anderson et al., 1991; Zotov et al., 2018), Ryzhenko-Bryzgalin (RB) model (Borisov and Shvarov, 1992; Tagirov and Seward, 2010; Shvarov, 2015), and Akinfiev-Diamond (AD) model (Akinfiev and Diamond, 2003).

In hydrothermal deposits, many trace elements, do not form their own pure solid phases but incorporate major minerals in isomorphic substitutions, which can be approximated by solid solution thermodynamic models. Generally, for an isostructural solid solution (A_xB_{1-x}) with mixing on one site and with *A* and *B* as the end-members (e.g., (Zn,Cd)S, (Mo,Re)S_2, Fe(As,$S)_2$), its standard molar Gibbs energy at given *T* and *P* is expressed as

$$\Delta G^0(A_xB_{1-x}) = x \times \Delta G^0(A) + (1-x) \times \Delta G^0(B) + \Delta G^0_{ideal} + \Delta G^0_{ex} \quad (18a)$$

where $\Delta G^0(A)$ and $\Delta G^0(B)$ are the standard molar Gibbs energies of the pure end-member *A* and *B*, *x* is the mole fraction of end-member *A*; these two terms of equation (18a) correspond to mechanical mixing of A and B. The mixing energy of the solution is composed of ΔG^0_{ideal} which is a Gibbs energy of ideal chemical mixing of random distribution with no preferred energetics, and ΔG^0_{ex} which is excess energy accounting for non-ideality of mixing (non-random distribution of A and B in the site and specific chemical interactions). For the simplest case of ideal mixing (1 site, 2 compounents)

$$\Delta G^0_{ideal} = RT(x_A \ln x_A + (1-x_A)\ln(1-x_A)) \quad (18b)$$

or more generally for *i* components

$$\Delta G^0_{ideal} = RT \sum x_i \ln x_i \quad (18c)$$

For multiple-site mixing (such as often in silicates) the equation becomes

$$\Delta G^0_{ideal} = RT \sum m_j \sum x_{ij} \ln x_{ij} \quad (18d),$$

where m_j is the number of j sites and x_{ij} is mole fraction of i in site j. The ΔG^0_{ideal} term is always negative because $0 \leq x_i \leq 1$, making the solution stable compared to a mechanical mixture (see Powell, 1976). The ΔG^0_{ex} term can be negative or positive depending on the mixing energetics. The reader can find in the literature different models for ΔG^0_{ex} (and its composing entropy and enthalpy terms analogous to equation 15) implemented in computer codes for specific non-ideal systems (e.g., various regular and subregular solution models, Margules, Redlich-Kister and other equations). For the major silicate and oxide minerals in the high-temperature magmatic and metamorphic domains, these models were applied for both cationic (e.g., Na, K, Ca, Mg, Fe, Mn, Ti) and anionic (Al, Si, OH, F, Cl) sites (as detailed in Grover, 1976; Navrotsky, 1987; Wood, 1987; Holland and Powell, 1998; to name a few). In contrast, such models are much less developed for trace elements in hydrothermal sulfide or oxide ore minerals. As a result, in a first approximation, ideal solid solutions with $\Delta G^0_{ex} = 0$ (and $a = x$ in equation (6)) can be adopted for minor element substitutions in sulfides and oxides. This approach has been used, for example, to calculate metal concentrations in the fluid in equilibrium with their solid solution mineral phase, such as Ge in quartz (Pokrovski and Schott, 1998) or Cd in sphalerite (Bazarkina et al., 2010). Non-ideal solid-solution models (with $\Delta G^0_{ex} \neq 0$, and therefore $a \neq x$) based on experimental or theoretical data were proposed for Au and Ag in electrum (Pal'yanova, 2008) and for As in arsenian pyrite (Xing et al., 2019). The solid-solution models above require knowledge of Gibbs energy of the end-member phases. In many cases, however, the corresponding trace element end-member phase is unstable, poorly known or of different stoichiometry from the major-element end-member. This is the case, for example, of Ge^{IV} or In^{III} in sphalerite or Au^{I} in arsenian pyrite whose incorporation occurs via charge compensation, structural vacancies or special coordination environments that differ from the stoichiometry of the major element end-member. The thermodynamic description of such types of substitution requires knowledge of the exact metal speciation and solubility in the solid phase that can be obtained by combining spectroscopic analyses, molecular simulations, and fluid-mineral partitioning measurements (e.g., Pokrovski et al., 2021a; Liu et al., 2023) – approaches that are still in their infancy.

More detailed account of the thermodynamic equations of state for minerals, gases and aqueous species is beyond the scope of this introductory article and can be found in extended reviews (e.g., Navrotsky, 1987; Oelkers et al., 2009; Stefánsson et al., 2013) and seminal books (e.g., Garrels and Christ, 1965; Fraser, 1976; Wood and Fraser, 1977; Anderson, 2005).

4.2. Thermodynamic databases and computer codes

Thermodynamic functions for aqueous and gaseous species and solid phases can nowadays be accessed from thermodynamic databases (e.g., SUPCRT, SUPCRTBL, MINTEQ, LLNL). These databases are integrated in computer codes allowing thermodynamic equilibrium calculations in multicomponent fluid-mineral-gas systems at elevated temperatures and pressures (e.g., EQ3/6, CHESS, HCh, PHREEQC, GEM, GWB). Detailed account of the existing databases, associated software, and advantages and limitations of the thermodynamic models for aqueous species and minerals may be found in Oelkers et al. (2009) and Pokrovski et al. (2025). Table 4 lists non-exhaustively the most frequently used databases and computer codes for modeling fluid-mineral(-gas) interactions in the systems of geochemical interest. The

use of one or another code is mostly a matter of habit, accessibility (different computer platforms or licensing), and the *T-P* range covered by calculations, as well as the choice of elements, species, and solid phases. For example, the MINTEQ and PHREEQC codes and their original databases were suitable for relatively low-temperature calculations (≤300 °C). In contrast, the EQ3/6, HCh and GEM programs allow mineral-fluid equilibrium calculations up to high-temperature magmatic and high-pressure metamorphic conditions by combining HKF-model revised and improved databases (e.g., Huang and Sverjensky, 2019). Perple_X is primarily designed for modeling mineral phase diagrams under metamorphic conditions and includes a large set of silicate mineral solid solutions, but offers a limited selection of aqueous species. To enable a more detailed assessment of the solubility speciation in metamorphic systems while preserving the accuracy of mineral composition predictions by Perple_X, it can be complemented by codes such as HCh offering a flexibility of fluid-phase models and a large choice of aqueous species (e.g., He et al., 2024). Modern computer tools make it possible to link or exchange databases to allow equilibrium calculations, e.g. by the PHREEQC code using the SUPCRTBL thermodynamic database, greatly extending the *T-P* range of the original software (e.g., Hang et al., 2020). Whatever the exact computer code, its general structure is quite similar, as shown in Figure 3. Each calculation requires the preparation of a set of input files describing the composition of the system to be modeled in terms of i) minerals and species (and gases) to be considered, ii) the initial system solid phase and fluid chemical constituents and their amounts and concentrations and, eventually, iii) a description of the *T-P* path, mixing scheme, variation in fluid/rock ratio or other instructions. The format of those files may vary from one code to another. Once these files are created, they are used by the code, along with standard Gibbs energies or reaction constants calculated from the associated thermodynamic databases, to find the composition of the equilibrium system at each programmed step. This search is made either using Gibbs energy minimization algorithms that search for the minimum of the sum of Gibbs energies of all species and phases by varying their activities (equations 6, 7 and 13) or by solving the system of equations (similar to equation 12). In both cases, mass and electrical charge balance are two additional fundamental constraints. The resulting output is a list of thermodynamically stable minerals with their respective amounts, and gas and aqueous species with their corresponding partial pressures and concentrations at equilibrium. Some codes also offer easy-to-use graphical interfaces that allow plots of species distribution or solid-phase equilibrium diagrams (e.g., GWB, Perple_X), while others provide easy-to-use digital text or Excel output files (e.g., HCh). Modern codes enable the passing of instructions defining a *T-P* path, mixing schemes of different reservoirs. Such options greatly facilitate calculations as a function of *T* and *P*, and the fluid/rock ratio. Other options offer a possibility of programming different steps in the system evolution, e.g., first by equilibrating a fluid with a rock and then allowing the fluid separation and subsequent evolution. They also allow modeling of progressive fluid-rock interactions by the so-called flow-through reaction technique, in which an aqueous solution percolates through a rock defined by a series of reactors of variable bulk composition, defined in terms of pre-reacted rock and solution (e.g., Shvarov and Bastrakov, 1999). Examples of such types of modeling of fluid evolution in metamorphic and sea-floor hydrothermal settings can be found in Zhong et al. (2015), Petrella et al. (2021) or Hurtig et al. (2024). Since pioneering work in the 1990s (e.g., Steefel and Lasaga, 1994), there is nowadays a growing body of studies of reactive transport calculations applied to hydrothermal deposits that integrate, along with the thermochemistry aspects discussed above, reaction rate constants for major silicate minerals with fluid flow physical parameters, to enable modeling of ore deposition in space and time (e.g., Chang et al., 2024; references therein).

4.3. Examples of modeling related to ore deposit formation

The thermodynamic modeling approaches for fluid-rock interactions outlined above have been applied to a number of general and specific cases of ore deposit formation in various hydrothermal-metamorphic-sedimentary contexts. These include geothermal settings (e.g., Simmons et al., 2016; Stefánsson et al., 2016), deep-sea hydrothermal systems (Melekestseva et al., 2017; Hurtig et al., 2024), porphyry-epithermal deposits (e.g., Heinrich, 2005; Kouzmanov and Pokrovski, 2012; Pokrovski et al., 2015; Chang et al., 2024), sedimentary-basin hosted deposits (e.g., Barré et al., 2017; Vallance et al., 2024), and orogenic gold deposits (e.g., Rauchenstein-Martinek et al., 2014; Zhong et al., 2015; Petrella et al., 2021) to name a few. Two examples of the capabilities and research impact of the method are briefly discussed below, with a focus on gold deposits.

Porphyry-epithermal deposits. Figure 4 shows an example of thermodynamic modeling of magmatic fluid evolution in a typical context of porphyry-epithermal Cu-Au(-Mo) deposits. These settings are particularly amenable to such modeling because of the extensive geological and mineralogical knowledge of these systems and the abundance of fluid inclusion data that allow the modeler to place robust constraints on the initial fluid composition and its *T-P* evolutionary path (e.g., Heinrich, 2005). Chemical equilibrium calculations shown in Fig. 4 simulate the cooling of a sulfur- and Cu-Fe-Au-bearing magmatic fluid along a typical *T-P* gradient in equilibrium with aluminosilicate rocks. First, these calculations quantitatively confirm the common mineral associations and precipitation sequences of the major sulfide and oxide copper and iron ore minerals observed in porphyry settings. In addition, they allow quantitative estimation of changes in Cu, Fe, and Au contents of the fluid upon cooling, greatly aiding in the interpretation of natural fluid inclusion data (Kouzmanov and Pokrovski, 2012). The general results of the modeling is to demonstrate that cooling of a magmatic metal- and sulfur-bearing fluid is the main cause of Cu and Fe precipitation. A more specific result is to highlight the role played by the recently discovered sulfur aqueous species – trisulfur radical ion ($S_3^{\bullet-}$) – in complexing and transporting gold in the fluid phase. Indeed, calculations show that most Au in S-rich porphyry fluids at temperatures above 400 °C is transported as the $Au(HS)S_3^-$ complex. Its predicted concentrations in equilibrium with metallic gold at such conditions are in excellent agreement with Au contents measured in fluid inclusions (up to 10 ppm Au; Table 3). In contrast, the concentrations of traditional Au hydrosulfide and chloride complexes are 10 to 100 times lower. These results, which can only be achieved by numerical modeling, imply that the $S_3^{\bullet-}$ ion is a key player in the process of Au extraction from hydrous sulfur-rich magmas in arc settings (Pokrovski et al., 2015; He et al., 2024). It is only in the epithermal environment, below ~300 °C, that the "traditional" hydrosulfide complex, $Au(HS)_2^-$, takes over from $Au(HS)S_3^-$ in the transport of gold (Fig. 4). Overall, the modeling demonstrates that the capacities to transport gold by S-rich sulfide-sulfate(or SO_2) bearing fluids at circa-neutral pH buffered by felsic rocks, are very high over a large temperature range. Note that the currently available thermodynamic datasets and models allow achieving such degree of detail in modeling of fluid-rock interactions only for liquid-like fluids with densities above ~0.4 g/cm^3 (Fig. 1 and section 2.2). Vapor-like fluids in porphyry settings, which are either produced by direct magma degassing at shallow levels or by unmixing of supercritical saline fluids upon their cooling and decompression (e.g., Heinrich et al., 1992; Sillitoe, 2010), are not yet amenable to a similar degree of quantification for most metals for the two reasons often ignored by geologists practicing thermodynamic modeling using available computer codes. First, the metal speciation in such low-density phases is fundamentally different from that in the liquid and is much poorer known, resulting in a lack of well-constrained vapor-phase species stoichiometries and thermodynamic functions. Second, the widely-used thermodynamic models for aqueous species (such as HKF) are not applicable to such low densities and may lead to large errors and, sometimes, unphysical speciation for both sulfur and metals. Semi-

quantitative estimations of bulk Au, Cu and Fe partitioning between shallow-depth silicate melts and magmatic vapors or between brine and vapor phases can be made on the basis of experimentally measured partition coefficients for metals and empirical density and hydration models proposed (e.g., Pokrovski et al., 2013a for a review).

Sediment-hosted hydrothermal deposits. Another example, shown in Figure 5, illustrates fluid interactions with organic-bearing sedimentary rocks leading to the formation of sediment-hosted gold and associated metal ore deposits. Gold in sediment- and metamorphic rock-hosted deposits is frequently associated with organic matter or its metamorphosed products such as pyrobutimen or graphite (C_{org}). Organic matter has generally been thought to play a major role in scavenging gold from the fluid (e.g., Robb and Meyer, 1995). Indeed, dissolution of organic carbon, because of its reducing nature, should increase the activity of H_2 in the fluid. This increase should shift the equilibrium of reaction (2a) to the right favoring gold precipitation. However, the reactions of an aqueous fluid with organic matter are also accompanied by changes in other reaction (2a) components, such as H_2S and H^+. Consequently, the resulting effect on Au solubility can only be quantified by multi-component chemical equilibrium simulations. In Fig. 5, an oxidized, moderately saline and sulfate-bearing fluid of magmatic origin, carries Au, As and Fe in concentrations as commonly found in fluid inclusions from epithermal high-sulfidation Cu-Au deposits (1, 100 and 1000 ppm, respectively, Kouzmanov and Pokrovski, 2012). Such fluids are often acidic due to the hydrolysis of magmatic SO_2 to sulfuric acid (e.g., Heinrich, 2005) and a lack of reactive alkali aluminosilicate rocks or carbonates that could buffer the fluid pH in the context of the selected sandstone-dominated sedimentary environment (Vallance et al., 2024). This fluid interacts, at typical *T-P* conditions of 300 °C and 500 bar, with a C_{org}-bearing sandstone, at increasing content of organic carbon (approximated by a C/H ratio of 1, see details in the Fig. 5 caption). The fluid is saturated with metallic gold and pyrite through the whole interaction process to allow direct estimation of the fluid transporting capacity for Au, Fe and S. In addition to the ability to model precipitation and dissolution of pure minerals (as in Fig. 4), arsenic incorporation in pyrite as a solid solution with sulfur, $Fe(S,As)_2$, can also be quantified using a recent thermodynamic model for arsenian pyrite solid solution (Xing et al., 2019). It can be seen in Fig. 5a that the fluid interaction with C_{org} results in contrasting behavior of the three metals. Iron concentrations drop by as much as 8 orders of magnitude in the presence of low C_{org} levels in the rock (<2 mol %). Arsenic concentrations remain constant in the fluid, and only a small fraction is incorporated into pyrite at tenors of few ppm As. It is only when the aqueous sulfate is nearly consumed by reduction with organic carbon (C_{org} in rock >3 mol %) that arsenic is incorporated into pyrite in amounts comparable to the naturally observed levels (1000s ppm As) found in many epithermal and low-grade metamorphic deposits characterized by the ubiquitous presence of arsenian pyrite (e.g., Reich et al., 2005). In contrast, gold shows a spectacular increase in solubility, reaching several 100s ppm Au at carbon contents in the system comparable to that of sulfur (at C_{org} >2–3 mol %), followed by a slight decrease (to 10s ppm Au) when approaching graphite saturation. These contrasting changes are fundamentally driven by the concomitant evolution of pH and redox of the sulfate-bearing fluid, which are controlled by thermochemical sulfate reduction (TSR) reactions:

$$SO_4^{2-} + CH_{4(aq)} + 2\ H^+ = H_2S_{(aq)} + CO_{2(aq)} + 2\ H_2O_{(l)} \quad (19)$$

$$CH_{4(aq)} + 2\ O_{2(g)} = CO_{2(aq)} + 2\ H_2O_{(l)} \quad (20)$$

It follows from these reactions, and the more detailed quantitative evolution of its constituent concentrations shown in Fig. 5b,c, that the increase in pH and H_2S during the TSR has a much stronger effect on Au solubility as controlled by reaction (2a) than the decrease in O_2 (equivalent

to increase in H_2, reaction (4)). The overall effect of these changes results in strongly promoting Au solubility rather than its precipitation. This finding of a positive effect of C_{org} on Au transport, which could only be obtained by numerical modeling, challenges the old paradigm that organic matter exclusively plays a scavenger role for Au, owing to a generally reducing nature of C_{org}. The model shown in Fig. 5 has recently been used in combination with geochemical, mineralogical and structural geology approaches, to interpret Au transport and accumulation in an ancient petroleum basin in a case study of the Shahuindo gold epithermal deposit hosted within the Marañón fold and thrust belt of northern Peru (Vallance et al., 2024; Galdos et al., 2024). Given the ubiquity of graphite and arsenian pyrite in many sediment-hosted gold deposits, the great potential of thermodynamic modeling demonstrated here should be exploited for many other deposits worldwide.

5. Caveats and limitations of the thermodynamic modeling approach

It has been shown in this overview that the thermodynamic modeling approach for fluid-rock interactions can be a valuable complement to traditional methods in the domain of georessources. It can serve case studies in a given ore deposit context as well as the more general understanding of physical-chemical phenomena of fluid-rock interactions and major factors of ore deposit formation inaccessible by experimental or naturalistic approaches alone. However, it has its own specific limitations and caveats that are briefly outlined as follows.

The major caveat when applying this approach to a given natural setting is to know the composition and *T-P* path of the system; this knowledge may be greatly variable from one case to another and for different ore deposit types. Therefore, detailed geodynamic, mineralogical, geochemical and fluid-inclusion information should be acquired before attempting such a modeling.

The second major caveat is the degree of completeness when defining the physical-chemical system to be modeled. For example, omission, in the system description input files or default databases, of important minerals such as pyrite might simply lead to unrealistic equilibrium mineral associations, such as pyrrhotite and hematite or formation of unphysically sulfur-rich fluids, to satisfy sulfur and iron mass balance in the program. Similarly, omission/absence of major charge-bearing species to be included in the fluid, such as Na^+, K^+ and Cl^-, would force the program to seek to satisfy the electrical charge and mass balance at equilibrium by artificially increasing activities of nominally minor species (e.g., metal cations), changing significantly the fluid pH or precipitating naturally unrealistic Na-bearing minerals.

For minor and trace metals that contribute little to the system mass balance, omitting their dominant aqueous complexes, such as $Au(HS)S_3^-$ or $CuCl_2^-$ (see Table 2 for the major species), would lead to significant underestimation of dissolved metal content in the fluid at equilibrium (e.g., Fig. 4). Conversely, inclusion of complexes without molecular or spectroscopic evidence and well constrained thermodynamic properties can lead to large overestimates of metal concentrations. For example, using the HKF parameters of the tetrasulfide Au complex $Au(HS)(H_2S)_3^0$ (Loucks and Mavrogenes, 1999), would yield gold solubilities of ~10^4 times higher than those predicted in Table 2 or found in natural fluid inclusions from high-sulfidation epithermal deposits. Another appealing example is platinum and palladium (and other PGE) whose solubility predictions in hydrothermal fluids use default

databases such as SUPCRT92 or SUPCRTBL that include only hydroxide, sulfate and chloride species. Such default calculations return unphysically small Pt and Pd solubilities (less than 1 atom per kg of fluid) in typical epithermal fluids. This is because they disregard the key hydrosulfide and trisulfur ion complexes whose stability was constrained in recent work (e.g., Filimonova et al., 2021; Pokrovski et al., 2021b, Laskar et al., 2022, 2025; references therein). Indeed, inclusion of these sulfur complexes yields Pt and Pd solubilities of ppb-to-ppm levels, in line with multiple instances of PGE remobilization and concentration in hydrothermal settings.

As discussed in section 2.2, the degree of robustness of the thermodynamic data for such species and the extent of the *T-P* range over which the data can be extrapolated with confidence are the major contributions to the uncertainties of metal solubility estimates. Therefore, care should be taken particularly when using default databases often supplied with the programs listed in Table 4, or tentative sets of HKF parameters from certain studies (e.g., see Pokrovski et al., 2024). For example, if equilibrium calculations for typical hydrothermal fluids as such those listed in Table 1 return dominant metal species other than those listed in Table 2, the original thermodynamic data source should be carefully re-considered. This is, however, not an easy exercise because many thermodynamic databases do not directly report original data sources, in the best case just referring to previous thermodynamic compilations. The modeler has therefore to dig into the literature to find the original experimental or theoretical papers reporting thermodynamic properties for the aqueous species in question at elevated temperatures and pressures, and to incorporate them in the right form depending on the thermodynamic code (e.g., K or G^0 values, HKF coefficients).

Finally, if even with the current metal species data set, the calculated concentrations are still significantly (i.e. several log units) lower than natural fluid inclusion analyses, the user should first revise the initial conditions and the assumed concentrations of the key fluid components contributing to mineral solubility (e.g., redox, H_2S, pH, see reaction (2a,b)). If the agreement with nature is still insufficient, it is possible that other, as yet unknown, species dominate the metal speciation under the modeled conditions. For example, this was likely the case for molybdenum whose published stability constants of oxyhydroxide and oxysulfide complexes invoked in few existing studies (e.g., $HMoO_4^-$, $NaHMoO_4^0$, $MoO_2S_2^{2-}$) were largely insufficient to account for the high Mo concentrations analyzed in fluid inclusions from porphyry-epithermal systems (Kouzmanov and Pokrovski, 2012). Thus, other as yet unknown Mo species are likely to control molybdenum transport under these conditions. The generation of their thermodynamic parameters requires new experimental data.

Thus, the modeling of fluid-rock interactions for mineral resource studies is not an isolated approach. Rather, it is a continuous back-and-forth between computational results and what is observed in a given natural context, by re-adjusting the choice of initial system composition and solubility controlling parameters, and re-examining thermodynamic data sources for species and minerals. Other current major limitations of the fluid-rock modeling that include extending the *T-P*-density space (Fig. 1), acquiring new thermodynamic data (Table 2), understanding speciation of trace elements in major minerals, and linking chemical speciation with fluid flow physics, are briefly outlined below.

6. Perspectives and challenges

A major challenge in our modeling of geological fluids across the crustal *T-P* conditions is to develop a common framework of physical-chemical equations of state enabling predictions of thermodynamic properties of aqueous species from aqueous solutions to hypersaline brines and low-density vapor phases (Fig. 1). At present, there is a gap in our ability to predict metal behavior in multi-phase systems between, on the one hand, the liquid or relatively dense supercritical fluid phase (ρ > 0.4–0.5 g/cm^3) for which robust thermodynamic models (e.g., HKF or density model) are available and, on the other hand, the low-density under-saturated vapor (ρ < 0.01 g/cm^3) for which ideal gas thermodynamics may be applied with good accuracy. In between, lies a large domain of hydrothermal-magmatic vapors of intermediate density (<0.1–0.4 g/cm^3) in which metal speciation is still poorly known. Models applicable to this domain (e.g., hydration, density model) require far more extensive experimental data to reach an accuracy comparable to what we presently have for a higher density solution (HKF model) or a very low density gas phase (ideal gas anhydrous species equilibria). Some promising models for the vapor-liquid interface have been proposed (e.g., Akinfiev and Diamond, 2003), but they still lack the experimental data necessary for their parameterization. Another type of geological fluids, termed mixed H_2O-CO_2, typical of deep metamorphic contexts, has received little attention from thermodynamic modeling (e.g., Newton and Manning, 2009; Manning et al., 2013). HKF-based approaches that take into account the change of aqueous fluid dielectric constant in the presence of CO_2 have provided recent advances in modeling of metamorphic gold deposit formation (e.g., Kokh et al., 2017). However, for many metals, they still rely heavily on knowing the exact aqueous species involved. Similarly, recent estimates of the dielectric constant of water in the high *T-P* region of subduction zone fluids have recently allowed the computational capabilities of the traditional HKF model to be extended to pressures of several tens of kbars (e.g., Sverjensky et al., 2014; Huang and Sverjensky, 2019). However, experimental data on the speciation of most economic metals under such conditions are urgently needed to validate such predictions and to assess their uncertainties. Finally, linking thermodynamic equilibrium models of silicate melts to those of aqueous fluids is a formidable challenge, both from the point of view of thermodynamic concepts that differ between melts and fluids, and from the point of view of software algorithms and databases (e.g., Dingwell et al., 2022).

In the 2000s, molecular modeling approaches based on density functional theory (DFT), such as static quantum chemistry and first-principles molecular dynamics (FPMD), have provided insights into the atomic structure and hydration energy of ore-metal complexes (e.g., Au, Cu, Ag, Zn, Cd, Sb, Pt), helping to interpret spectroscopic and solubility data and to choose among possible speciation models to describe experimental data (e.g., Brugger et al., 2016; Pokrovski et al., 2013b, 2022a). In principle, modern FPMD methods enable calculations of Gibbs energies of complexation reactions for relatively simple metal complexes at virtually any temperature and pressure (e.g., Mei et al., 2014; Laskar et al., 2022; and numerous references therein). Although the realistic uncertainties associated with such calculations are still much greater than those from direct experimental measurements (where available), the situation is rapidly improving with advances in the computational power of molecular modeling, for which one of the main limitations is the prohibitively long duration of simulations. In the meantime, acquiring new experimental data (solubility and speciation) for aqueous complexes of many critical elements in hydrothermal fluids (e.g., Mo, Re, W, PGE, Co, In, Sc, Nb, Ta) remains the primary necessity to be able to integrate them in models of hydrothermal fluid-rock interactions.

Many economically valuable trace elements, however, do not commonly form their own mineral phases. Instead, they are hosted by major sulfide, oxide or silicate minerals (e.g., pyrite, chalcopyrite, magnetite, micas, serpentines) as isomorphic substitutions or complexes, clusters

and nanophases in the crystallographic structure and its defects. Therefore, there is a large unexplored domain of computational geochemistry of trace elements that awaits thermodynamic and kinetic information on their incorporation mechanisms, partition coefficients, and chemical and redox speciation in major minerals under hydrothermal conditions. The situation contrasts with the environmental geochemistry domain where large databases of trace metal speciation and sorption properties on the surfaces of major mineral phases are available (e.g., Stumm and Morgan, 1996), and with the magmatic and metamorphic petrology domain that widely uses solid solution models for a large range of lithophile elements in silicate minerals. Only few analogous models are currently operational for hydrothermal sulfide minerals. For example, it is only recently that a model of arsenic incorporation in arsenian pyrite could be integrated into existing thermodynamic codes (such as HCh, Xing et al., 2019; Fig. 5). A combination of hydrothermal experiments and high-resolution spectroscopy allowed the understanding of arsenic-controlled gold substitution mechanisms in pyrite and arsenopyrite in terms of gold-arsenic-sulfur sites formed in the mineral structure ($AuAs_nS_{6-n}$). These data have been placed into a quantitative thermodynamic framework, for the first time, in terms of equilibrium constant values of a reaction between gold species in the fluid and mineral (Pokrovski et al., 2021a). Analogous thermodynamic models are eagerly awaited for many economically critical trace elements (e.g., PGE, Ge, Ga, In, Tl, Te, Co) for which pyrite and other major iron, zinc and copper sulfarsenides are the principal hosts in hydrothermal deposits.

Another advance of the beginning of the 21th century is the growing application of physical hydrology approaches based on heat distribution, fluid flow models and permeability changes. Such approaches have allowed integrated reactive transport modeling of fluid paths, pressure and temperature evolution, unmixing and boiling, and three-dimensional ore distribution and shape (e.g., Ingebritsen and Appold, 2012; Weis et al., 2012; Stoltnow et al., 2023). However, the chemistry of fluid-rock interactions, mineral solubility, and chemical element speciation in the fluid and vapor phases are not yet quantitatively and systematically considered in these physical models, especially for economic metals. The integration of both chemistry and physics into the same conceptual model would thus be another major challenge for theoretical geochemistry and would contribute to our fundamental understanding of the role of fluid phases in ore deposit formation as well as to improving ore exploration and extraction.

Acknowledgments

This overview was motivated by the author's courses delivered for Master students in different universities for more than 20 years, as well as by the results of research of his team on metals and volatiles in hydrothermal fluids supported by funding from Agence National de la Recherche (grants SOUMET ANR-2011-Blanc-SIMI-5-6/009-01, and RadicalS ANR-16-CE31-0017), Institut des Sciences de l'Univers of the CNRS (INSU-CNRS), Mission pour les initiatives transverses et interdisciplinaires (MITI) - interdisciplinary programs of the CNRS MetalloMix 2021 (grant PtS3), and Conditions Extremes 2024 (grant ExtremeS), Institut Carnot ISIFoR (grants OrPet and AsCOCrit), Université de Toulouse (grant CO2MET), and French Ambassy. The author thanks L. Meinert, G. Beaudoin, and B. Lehmann for suggestions on previous versions of this paper, H. Chen for editorial handling, and two anonymous reviewers for their comments.

7. References

Akinfiev, N.N., Diamond, L.W., 2003. Thermodynamic description of aqueous nonelectrolytes over a wide range of state parameters. Geochim. Cosmochim. Acta 67, 613–627.

Akinfiev, N.N., Tagirov, B.R., 2014. Zn in hydrothermal systems: Thermodynamic description of hydroxide, chloride, and hydrosulfide complexes. Geochem. Intl. 52(3), 197–214.

Akinfiev, N.N., Zotov, A.V., 2001. Thermodynamic description of chloride, hydrosulphide, and hydroxide complexes of Ag(I), Cu(I), and Au(I) at temperatures of 25–500 °C and pressures of 1–2000 bar. Geochem. Intl. 39, 990–1006.

Anderson, G.M., 2005. *Thermodynamics of Natural Systems*. Cambridge University Press.

Anderson, G.M., Castet, S., Schott, J., Mesmer, R.E., 1991. The density model for estimation of thermodynamic parameters of reactions at high temperature and pressure. Geochim. Cosmochim. Acta 55, 769–1779.

Baes, C.F., Mesmer, R.E., 1976. *The Hydrolysis of Cations*. Wiley, New York, USA.

Barnes, H.L., 1997. *Geochemistry of Hydrothermal Ore Deposits*. Wiley, New York.

Barré, G., Truche, L., Bazarkina, E.F., Michels, R., Dubessy, J., 2017. First evidence of the trisulfur radical ion S_3^- and other sulfur polymers in natural fluid inclusions. Chem. Geol. 462, 1–14.

Bazarkina, E.F., Pokrovski, G.S., Zotov, A.V., Hazemann, J.-L., 2010. Structure and stability of cadmium chloride complexes in hydrothermal fluids. Chem. Geol. 276, 1–17.

Bazarkina, E.F., Pokrovski, G.S., Hazemann, J.-L., 2014. Structure, stability and geochemical role of palladium chloride complexes in hydrothermal fluids. Geochim. Cosmochim. Acta 146, 107–131.

Bénézeth, P., Diakonov, I., Pokrovski, G.S., Dandurand, J.-L., Schott, J., Khodakovsky, I.L., 1997. Gallium speciation in aqueous solution. Experimental study and modelling. Part II. Solubility of αGaOOH in acidic solutions from 150 to 250°C and hydrolysis constants of gallium (III) to 300°C. Geochim. Cosmochim. Acta 61, 1345–1357. https://doi.org/10.1016/S0016-7037(97)00012-4

Borisov, M.V., Shvarov, Y.V., 1992. *Thermodynamics of Geochemical Processes*. Moscow State University Publishing House, Moscow, 254 p. (in Russian).

Brimhall, G.H., Crerar, D.A., 1987. Ore fluids: Magmatic to supergene. Rev. Miner. 17, 235–321.

Brugger, J., Liu, W., Etschmann, B., Mei, Y., Sherman, D.M., Testemale, D., 2016. A review of the coordination chemistry of hydrothermal systems, or do coordination changes make ore deposits? Chem. Geol. 447, 219–253.

Chang, C., Xiao, K., Feng, G., Sun, L., Yang, J., 2024. Reactive transport numerical modeling of intermediate sulfidation epithermal deposit: A case study of Haopinggou Ag-Au-Pb-Zn deposit, Henan province, China. J. Geochem. Explor. 263, 107500.

Chase, M.W., Jr., Davies, C.A., Downey, J.R., Jr, Frurip, D.J., McDonald, R.A., Syverud, A.N., 1985. JANAF thermochemical tables, 3rd edition. J. Phys. Chem. Ref. Data 14, Suppl. 1.

Colin. A., Schmidt, C., Pokrovski, G.S., Wilke, M., Borisova, A.Y., Toplis, M., 2020. *In situ* determination of sulfur speciation and partitioning in aqueous fluid-silicate melt systems. Geochem. Persp. Let. 14, 31–35.

Crerar, D.A., Wood, S.A., Brantley, S., Bocarsly, A., 1985. Chemical controls on solubility of ore forming minerals in hydrothermal solutions. Can. Mineral. 23, 333–352.

Dadze, T.P., Kashirtseva, G.A., Novikov, M.P., Plyasunov, A.V., 2018. Solubility of calcium molybdate in aqueous solutions at 573 K and thermodynamics of monomer hydrolysis of Mo(VI) at elevated temperatures. Monatsh. Chem. 149, 261–282.

Diakonov I., Pokrovski G.S., Benezeth P., Schott J., Dandurand J.-L., Escalier J. (1997) Gallium speciation in aqueous solution. Experimental study and modelling. Part I. Thermodynamic properties of $Ga(OH)_4^-$ to 300°C. Geochim. Cosmochim. Acta 61, 1333–1343. https://doi.org/10.1016/S0016-7037(97)00011-2

Dirk, J.M., 2019. CHNOSZ: Thermodynamic calculations and diagrams for geochemistry. Front. Earth Sci., 16 July 2019, Sec. Geochemistry, Vol 7. https://doi.org/10.3389/feart.2019.00180

Dingwell, D.B., Henderson, G., Neuville, D.R., (eds), 2022. Geological Melts. Rev. Miner. Geochem. 87, 1–1088.

Fraser, D.G., ed., 1976. *Thermodynamics in Geology*. D. Reidel Publishing Company, Dordrecht, Holland.

Filimonova, O.N., Tagirov, B.R., Zotov, A.V., Baranova, N.N., Bychkova, Y.V., Tyurin, D.A., Chareev, D.A., Nickolsky, M.S., 2021. The solubility of cooperite PtS(cr) at 25 – 450 °C, Psat – 1000 bar and hydrosulfide complexing of platinum in hydrothermal fluids. Chem. Geol. 559, 119968.

Fontboté, L., Kouzmanov, K., Chiaradia, M., Pokrovski, G.S., 2017. Sulfide minerals in hydrothermal deposits. Elements 13, 97–103.

Galdos, R., Vallance, J., Baby, P., Salvi, S., Schirra, M., Velasquez, G., Viveen, W., Soto, R., Pokrovski, G.S., 2024. Origin and evolution of gold-bearing fluids in a carbon-rich sedimentary basin: a case study of the Algamarca epithermal gold-silver-copper deposit, northern Peru. Ore Geol. Rev. 166, 105857.

Gammons, C.H., Allin, N.C., 2022. Stability of aqueous Fe(III) chloride complexes and the solubility of hematite between 150 and 300 °C. Geochim. Cosmochim. Acta 330, 148–164.

Garrels, R., Christ, C., 1965. *Solutions, Minerals, and Equilibria*. Harper & Row.

Grover, J., 1976. Chemical mixing in multicomponent solutions: an introduction to the use of Margules and other thermodynamic excess functions to represent non-ideal behavior. In: *Thermodynamics in Geology* (Fraser, D.G., ed.), D. Reidel Publishing Company, Dordrecht, Holland.

Gysi, A.P., Hurtig, N.C., Pan, R., Miron, G.D., and Kulik, D.A., 2023. MINES thermodynamic database. New Mexico Bureau of Geology and Mineral Resources, version 23, https://doi.org/10.58799/mines-tdb .

Hang, G.R., Lu, P., Zhang, Y.L., Tu, K., Zhu, C., 2020. SupPHREEQC: A program to generate customized PHREEQC thermodynamic database based on Supcrtbl. Comput. Geosci. 143, 164560.

Hannington, M., Harðardóttir, V., Garbe-Schönberg, D., Brown, K.L., 2016. Gold enrichment in active geothermal systems by accumulating colloidal suspensions. Nat. Geosci. 9, 299–302.

He, D-Y., Qiu, K-F., Simon, A.C., Pokrovski, G.S., Yu, H., Connolly, J.A.D., Li, S., Turner, S., Wang, Q-F., Yang, M-F., Deng, J., 2024. Mantle oxidation by sulfur drives the formation of giant gold deposits in subduction zones. Proc. Nat. Acad. Sci. USA, 121(52), e2404731121. https://doi.org/10.1073/pnas.2404731121

Heinrich, C.A., 2005. The physical and chemical evolution of low-salinity magmatic fluids at the porphyry to epithermal transition: A thermodynamic study. Mineral. Dep. 39, 864–889.

Heinrich, C.A., Ryan, C.G., Mernagh, T.P., Eadington, P.J., 1992. Segregation of ore metals between magmatic brine and vapor - a fluid inclusion study using PIXE microanalysis. Econ. Geol. 87, 1566–1583.

Helgeson., H.C., Kirkham, D.H., Flowers, G.C., 1981. Theoretical prediction of the thermodynamic behavior of aqueous electrolytes at high pressures and temperatures: IV. Calculation of activity coefficients, osmotic coefficients, and apparent molal and standard and relative partial molal properties to 600°C and 5 kb. Amer. J. Sci. 291, 1249–1516.

Holland, T.J.B., Powell, R., 1998. An internally consistent thermodynamic data set for phases of petrological interest. J. Metamorph. Geol. 29, 333–383.

Holland, T.J.B., Powell, R., 2011. An improved and extended internally consistent thermodynamic dataset for phases of petrological interest, involving a new equation of state for solids. J. Metamorph. Geol. 29, 333–383.

Huang, F., Sverjensky, D.A., 2019. Extended Deep Earth Water model for predicting major element mantle metasomatism. Geochim. Cosmochim. Acta 254, 192–230.

Hurtig, N.C., Gysi, A.P., Monecke, T., Petersen, S., Hannington, M.D., 2024. Tellurium transport and enrichment in volcanogenic massive sulfide deposits: Numerical simulations of vent fluids and comparison to modern sea-floor sulfides. Econ. Geol. 119, 829–851.

Ingebritsen, S.E., Appold, M.S., 2012. The physical hydrology of ore deposits. Econ. Geol. 107, 559–584.

Johnson, J.W., Oelkers, E.H., Helgeson, H.C., 1992. SUPCRT92: A software package for calculating the standard molal thermodynamic properties of minerals, gases, aqueous species, and reactions from 1 to 5000 bar and 0 to 1000°C. Comput. Geosci. 18, 899–947.

Jolivet, J-P., Henry, M., Livage, J., 1994. *De la Solution à l'Oxyde*. InterEditions et CNRS Editions, Paris.

Kokh, M.A., Akinfiev, N.N., Pokrovski, G.S., Salvi, S., Guillaume, D., 2017. The role of carbon dioxide in the transport and fractionation of metals by geological fluids. Geochim. Cosmochim. Acta 197, 433–466.

Kouzmanov, K., Pokrovski, G.S., 2012. Hydrothermal controls on metal distribution in Cu(-Au-Mo) porphyry systems. In: Hedenquist JW, Harris M, Camus F (eds.), *Society of Economic Geologists Special Publication* 16, 573–618. https://doi.org/10.5382/SP.16.22

Laskar, C., Bazarkina, E.F., Kokh, M.A., Hazemann, J-L., Vuilleumier, R., Desmaele, E., Pokrovski, G.S., 2022. Stability and structure of platinum sulfide complexes in hydrothermal fluids. Geochim. Cosmochim. Acta 336, 407–422.

Laskar, C., Bazarkina, E.F., Pokrovski, G.S., 2025. The role of hydrosulfide complexes hydrogen sulfide in palladium transport and fractionation from platinum by hydrothermal fluids. Geochim. Cosmochim. Acta, in press. https://doi.org/10.1016/j.gca.2024.12.019

Liebscher, A., Heinrich, C.A., eds., 2007. Fluid-fluid interactions. Rev. Miner. Geochem. 65, 1–430.

Liu, W., McPhail, D.C., 2005. Thermodynamic properties of copper chloride complexes and copper transport in magmatic-hydrothermal solutions. Chem. Geol. 221, 21–39.

Liu, W., Etschmann, B., Mei, Y., Guan, Q., Testemale, D., Brugger, J., 2020. The role of sulfur in molybdenum transport in hydrothermal fluids: Insight from in situ synchrotron XAS experiments and molecular dynamics simulations. Geochim. Cosmochim. Acta 290, 162–179.

Liu., W., Mei, Y., Etschmann, B., Glenn, M., MacRae, C.M., Spinks, S.C., Ryan, C.G., Brugger, J., Paterson, D.J., 2023. Germanium speciation in experimental and natural sphalerite: Implications for critical metal enrichment in hydrothermal Zn-Pb ores. Geochim. Cosmochim. Acta 342, 198–214.

Loucks, R.R., Mavrogenes, J.A., 1999. Gold solubility in supercritical hydrothermal brines measured in synthetic fluid inclusions. Science 284, 2159–2163.

Manning, C.E., Shock, E.L., Sverjensky, D.A., 2013. The chemistry of carbon in aqueous fluids at crustal and upper-mantle conditions: Experimental and theoretical constraints. Rev. Miner. Geochem. 75, 109–148.

Manning, C.E., 2018. Fluids of the lower crust: deep is different. Annu. Rev. Earth. Planet. Sci., 46, 67–97.

Martell, A.E., Hancock, R.D., 1996. *Metal Complexes in Aqueous Solutions*. Plenum Press.

McKibben, M.A., Williams, A.E., Hall, G.E.M., 1990. Solubility and transport of platinum-group elements and Au in saline hydrothermal fluids: Constraints from geothermal brine data. Econ. Geol. 85, 1926–1934.

Mei, Y., Liu, W., Sherman, D.M., Brugger, J., 2014. Metal complexation and ion hydration in low density hydrothermal fluids: ab initio molecular dynamics simulation of Cu(I) and Au(I) in chloride solutions (25–1000 °C, 1–5000 bar). Geochim. Cosmochim. Acta 131, 196–212.

Melekestseva, I.Y., Maslennikov, V.V., Tret'yakov, G.A., Nimis, P., Beltenev, V.E., Rozhdestvenskaya, I.I., Maslennikova, S.P., Belogub, E.V., Danyushevsky, L., Large, R., Yuminov, A.M., Sadykov, S.A. (2017) Gold- and silver-rich massive sulfides from the Semenov-2 hydrothermal field, 13°31.13'N, Mid-Atlantic ridge: A case of magmatic contribution? Econ. Geol. 112, 741–773.

Migdisov, A., Williams-Jones, A.E., Brugger, J., Caporuscio, F.A., 2016. Hydrothermal transport, deposition, and fractionation of the REE: Experimental data and thermodynamic calculations. Chem. Geol. 439, 13–42. http://dx.doi.org/10.1016/j.chemgeo.2016.06.005

Miron, G.D., Wagner, T., Kulik, D.A., Heinrich, C.A., 2016. Internally consistent thermodynamic data for aqueous species in the system Na-K-Al-Si-O-H-Cl. Geochim. Cosmochim. Acta 187, 41–78.

Muffler, L.J.P., White, D.E., 1969. Active metamorphism of upper Cenozoic sediments in the Salton Sea Geothermal Field and the Salton Trough, South-Eastern California. Geol. Soc. Amer. Bull 80, 157–182.

Navrotsky, A., 1987. Models of crystalline solutions. Rev. Mineral. 17, 35–69.

Naumov, G.B., Ryzhenko, B.N., Khodakovsky, I.L., 1974. *Handbook of Thermodynamic Data*. US Geological Survey.

Newton, R.C., Manning, C.E., 2009. Hydration state and activity of aqueous silica in H_2O-CO_2 fluids at high pressure and temperature. Am. Mineral. 94, 1287–1290.

Oelkers, E.H., Bénézeth, P., Pokrovski, G.S., 2009. Thermodynamic databases for water-rock interaction. Rev. Miner. Geochem. 70, 1–46.

Pal'yanova, G., 2008. Physicochemical modeling of the coupled behavior of gold and silver in hydrothermal processes: Gold fineness, Au/Ag ratios and their possible implications. Chem. Geol. 255, 399–413.

Pearson, R.G., 1963. Hard and soft acids and bases. J. Amer. Chem. Soc. 85, 3533–3539.

Pearson, R.G., 1997. *Chemical Hardness*. Wiley.

Perfetti, E., Pokrovski, G.S., Ballerat-Busserolles, K., Majer, V., Gibert, F., 2008. Densities and heat capacities of aqueous arsenious and arsenic acid solutions to 350°C and 300 bar, and revised thermodynamic properties of $As(OH)_3^0$(aq), $AsO(OH)_3^0$(aq) and iron sulfarsenide minerals. Geochim. Cosmochim. Acta 72, 713–731.

Petrella, L., Thébaud, N., Evans, K., LaFlamme, C., Occhipinti, S., 2021. The role of competitive fluid-rock interaction processes in the formation of high-grade gold deposits. Geochim. Cosmochim. Acta 313, 38–54.

Pokrovski, G.S., Schott, J., 1998. Thermodynamic properties of aqueous germanium(IV) hydroxide complexes from 25 to 350°C: Implications for the behavior of Ge and the Ge/Si ratio in hydrothermal fluids. Geochim. Cosmochim. Acta 62, 1631–1642.

Pokrovski, G.S., Dubrovinsky, L.S., 2011. The S_3^- ion is stable in geological fluids at elevated temperatures and pressures. Science 331, 1052–1054.

Pokrovski, G.S., Dubessy, J., 2015. Stability and abundance of the trisulfur radical ion S_3^- in hydrothermal fluids. Earth Planet. Sci. Lett. 411, 298–309.

Pokrovski, G.S., Roux, J., Hazemann, J.-L., Testemale, D., 2005. An X-ray Absorption spectroscopy study of argutite solubility and germanium aqueous speciation in hydrothermal fluids to 500°C and 400 bar. Chem. Geol. 217, 127–145.

Pokrovski, G.S., Borisova, A.Y., Roux, J., Hazemann, J-L., Petdang, A., Tella, M., Testemale, D., 2006. Antimony speciation in saline hydrothermal fluids: A combined X-ray absorption fine structure spectroscopy and solubility study. Geochim. Cosmochim. Acta 70, 4196–4214.

Pokrovski, G.S., Borisova, A.Y., Bychkov, A.Y., 2013a. Speciation and transport of metals and metalloids in geological vapors. Rev. Miner. Geochem. 76, 165–218.

Pokrovski, G.S., Roux, J., Ferlat, G., Seitsonen, A., Vuilleumier, R., Hazemann, J-L., 2013b. Silver in saline hydrothermal fluids from in situ X-ray absorption spectroscopy and first-principles molecular dynamics. Geochim. Cosmochim. Acta 106, 501–523.

Pokrovski, G.S., Akinfiev, N.N., Borisova, A.Y., Zotov, A.V., Kouzmanov, K., 2014. Gold speciation and transport in geological fluids: insights from experiments and physical-chemical modeling. In: Garofalo P, Ripley E (eds.), *Gold-Transporting Fluids in the Earth's Crust*. Geol. Soc. London Spec. Publ. 402, 9–70.

Pokrovski, G.S., Kokh, M.A., Guillaume, D., Borisova, A.Y., Gisquet, P., Hazemann, J-L., Lahera, E., Del Net, W., Proux, O., Testemale, D., Haigis, V., Jonchière, R., Seitsonen, A.P., Ferlat, G., Vuilleumier, R., Saitta, A.M., Boiron, M-C., Dubessy, J., 2015. Sulfur radical species form gold deposits on Earth. Proc. Nat. Acad. Sci. USA 112(44), 13484–13489.

Pokrovski, G.S., Escoda, C., Blanchard, M., Testemale, D., Hazemann, J-L., Gouy, S., Kokh, M.A., Boiron, M-C., de Parseval, F., Aigouy, T., Menjot, L., de Parseval, P., Proux, O., Rovezzi, M., Béziat, D., Salvi, S., Kouzmanov, K., Bartsch, T., Pöttgen, R., Doert, T., 2021a. An arsenic-driven pump for invisible gold in hydrothermal systems. Geochem. Persp. Let. 17, 39–44.

Pokrovski, G.S., Kokh, M.A., Desmaele, E., Laskar, C., Bazarkina, E.F., Borisova, A.Y., Testemale, D., Hazemann, J-L., Vuilleumier, R., Ferlat, G., Saitta, A.M., 2021b. The trisulfur radical ion $S_3^{\bullet-}$ controls platinum transport by hydrothermal fluids. Proc. Nat. Acad. Sci. USA 118, e2109768118.

Pokrovski, G.S., Desmaele, E., Laskar, C., Bazarkina, E.F., Testemale, D., Hazemann, J-L., Vuilleumier, R., Seitsonen, A.P., Ferlat, G., Saitta, A.M., 2022a. Gold speciation in hydrothermal fluids revealed by in situ high energy resolution X-ray absorption spectroscopy. Am. Mineral. 107, 369–376.

Pokrovski G.S., Sanchez-Valle C., Guillot S., Borisova A.Y., Muñoz M., Auzende A-L., Proux O., Roux J., Hazemann J-L., Testemale D., Shvarov Y.V. (2022b) Redox dynamics of subduction revealed by arsenic in serpentinite. Geochem Persp Let 22:36–41.

Pokrovski, G.S., Wilke, M., Kokh, M.A., 2024. Artificially high stability of the sodium hydromolybdate ion pair in aqueous solution. Comment on Guan et al. (2023) Different metal coordination in sub- and super-critical fluids: Do molybdenum (IV) chloride complexes contribute to mass transfer in magmatic systems?", Geochim. Cosmochim. Acta 354, 240–251. Geochim. Cosmochim. Acta, 387, 130–132.

Pokrovski, G.S., Stefánsson, A.S., Kouzmanov, K., 2025. Sulfur in hydrothermal fluids. In: *The Role of Sulfur in Planetary Processes: from Cores to Atmospheres*. D. Harlov, G.S. Pokrovski (eds.), Springer Nature (accepted).

Powell, R., 1976. Activity-composition relationships for crystalline solutions. In: Thermodynamics in Geology (Fraser, D.G., ed.), D. Reidel Publishing Company, Dordrecht, Holland.

Rauchenstein-Martinek, K., Wagner, T., Walle, M., Heinrich, C.A., 2014. Gold concentrations in metamorphic fluids: a LAICPMS study of fluid inclusions from the Alpine orogenic belt. Chem. Geol. 385, 70–83.

Reich, M., Kesler, S.E., Utsunomiya, S., Palenik, C.S., Chryssoulis, S.L., Ewing, R.C., 2005. Solubility of gold in arsenian pyrite. Geochim. Cosmochim. Acta 69, 2781–2796.

Robb, L.J., Meyer, F.M., 1995. The Witwatersrand basin, South Africa: Geological framework and mineralization processes. Ore Geol. Rev. 10, 67–94.

Robie, R.A., Hemingway, B.S., 1995. Thermodynamic properties of minerals and related substances at 298.15 K and 1 bar (10^5 Pascals) pressure and at higher temperatures. U.S. Geological Survey Bulletin 2131, 1–461.

Rudnick, R.L., Gao, S., 2014. Composition of the continental crust. In: *Treatise on Geochemistry*, 2nd edition, 4, 1–51. http://dx.doi.org/10.1016/B978-0-08-095975-7.00301-6

Salvi, S., Pokrovski, G.S., Schott, J., 1998. Experimental investigation of aluminum-silica aqueous complexing at 300°C. Chem. Geol. 151, 51–67.

Saunier, G., Pokrovski, G.S., Poitrasson, F., 2011. First experimental determination of iron isotope fractionation between hematite and aqueous solution at hydrothermal conditions. Geochim. Cosmochim. Acta. 75, 6629–6654.

Shvarov, Y.V., 2015. A suite of programs, OptimA, OptimB, OptimC, and OptimS, compatible with the Unitherm database, for deriving the thermodynamic properties of aqueous species from solubility, potentiometry and spectroscopy measurements. Applied Geochem. 55, 17–27.

Shvarov, Y., Bastrakov, E., 1999. HCh: a software package for geochemical equilibrium modelling. User's Guide. Record 1999/25, Australian Geological Survey Organization, Canberra.

Sillitoe, R.H., 2010. Porphyry copper systems. Econ. Geol. 105, 3–41.

Simmons, S.F., Brown, K.L., Tutolo, B.M., 2016. Hydrothermal transport of Ag, Au, Cu, Pb, Te, Zn, and other metals and metalloids in New Zealand geothermal systems: spatial patterns, fluid-mineral equilibria, and implications for epithermal mineralization. Econ. Geol. 111, 589–618.

Steefel, C., Lasaga, A., 1994. A coupled model for transport of multiple chemical species and kinetic precipitation/dissolution reactions with applications to reactive flow in single-phase hydrothermal system. Am. J. Sci. 294, 529–592.

Stefánsson, A., Driesner, T., Bénézeth, P., (eds), 2013. *Thermodynamics of Geothermal Fluids*. Rev. Miner. Geochem. 76, 1–350.

Stefánsson, A., Keller, N.S., Gunnarsson-Robin, J., Kaasalainen, H., Björnsdóttir, S., Pétursdóttir, S., Jóhannesson, H., Hreggvidsson, G.Ó., 2016. Quantifying mixing, boiling, degassing, oxidation and reactivity of thermal waters at Vonarskard, Iceland. J. Volcan. Geotherm. Res. 309, 53–62.

Stoltnow, M., Weis, P., Korges, M., 2023. Hydrological controls on base metal precipitation and zoning at the porphyry-epithermal transition constrained by numerical modeling. Sci. Rep. 13, 3786.

Stumm, W., Morgan, J.J., 1996. *Aquatic Chemistry: Chemical Equilibria and Rates in Natural Waters*. 3rd Edn., Wiley & Sons, NJ, USA, 1022 p.

Sverjensky, D.A., Shock, E.L., Helgeson, H.C., 1997. Prediction of the thermodynamic properties of aqueous metal complexes to 1000 °C and 5 kb. Geochim. Cosmochim. Acta 61, 1359–1412.

Sverjensky, D.A., Harrison, B., Azzolini, D., 2014. Water in the deep Earth: The dielectric constant and the solubilities of quartz and corundum to 60 kb and 1200 °C. Geochim. Cosmochim. Acta 129, 125–145.

Tagirov, B.R., Schott, J., 2001. Aluminum speciation in crustal fluids revisited. Geochim. Cosmochim. Acta 65, 3965–3992.

Tagirov, B.R., Seward, T.M., 2010. Hydrosulfide/sulfide complexes of zinc to 250°C and the thermodynamic properties of sphalerite. Chem. Geol. 269, 301–311.

Tagirov, B.R., Filimonova, O.N., Trigub, A.L., Akinfiev, N.N., Nickolsky, M.S., Kvashnina, K.O., Chareev, D.A., Zotov, A.V., 2019. Platinum transport in chloride-bearing fluids and melts: insights from in situ X-ray absorption spectroscopy and thermodynamic modeling. Geochim. Cosmochim. Acta 254, 86–101.

Testemale, D., Brugger, J., Liu, W., Etschmann, B., Hazemann, J-L., 2009. In-situ X-ray absorption study of iron(II) speciation in brines up to supercritical conditions. Chem. Geol. 264, 295–310.

Trofimov, N.D., Tagirov, B.R., Akinfiev, N.N., Reukov, V.L., Nickolsky, M.S., Nikolaeva, I.Y., Tarnopolskaya, M.E., Afanasyev, A.A., 2023. Chalcocite Cu_2S solubility in aqueous sulfide and chloride fluids. Thermodynamic properties of copper(I) aqueous species and copper transport in hydrothermal systems. Chem. Geol. 625, 121413.

Yardley, B.W.D., Banks, D.A., Bottrell, S.H., Diamond, L.W., 1993. Post-metamorphic gold quartz veins from NW Italy –The composition and origin of the fluid. Miner. Mag. 57, 407–422.

Yardley, B.W.D., 2005. Metal concentrations in crustal fluids and their relationship to ore formation. Econ. Geol. 100th Anniv. Spec. Vol. 100, 613–632.

Vallance, J., Galdos, R., Balboa, M., Berna, B., Cabrera, O., Baya, C., Van De Vyver, C., Viveen, W., Béziat, D., Salvi, S., Brusset, S., Baby, P., Pokrovski, G.S., 2024. Combined effect of organic carbon and arsenic on the formation of sediment-hosted gold deposits: A case study of the Shahuindo epithermal deposit, Peru. Econ. Geol. 119, 85–112.

Wagman, D.D., et al., 1982. The NBS tables of chemical thermodynamic properties. Selected values for inorganic and C1 and C2 organic substances in SI units. J. Phys. Chem. Ref. Data. 11, supplement 2.

Wedepohl, H., 1995. The composition of the continental crust. Geochim. Cosmochim. Acta 59, 1217–1239.

Weis, P., Driesner, T., Heinrich, C.A., 2012. Porphyry-copper ore shells form at stable pressure-temperature fronts within dynamic fluid plumes. Science 338, 1613–1616.

Wood, B., 1987. Thermodynamics of multicomponent systems containing several solid solutions. Rev. Mineral. 17, 71–95.

Wood, B.J., Fraser, D.G., 1977. *Elementary Thermodynamics for Geologists*. Oxford University Press, Oxford.

Wood, S.A., Samson, I.M., 1998. Solubility of ore minerals and complexation of ore metals in hydrothermal solutions. Rev. Econ. Geol. 10, 33–80.

Xing, Y., Brugger, J., Tomkins, A., Shvarov, Y., 2019. Arsenic evolution as a tool for understanding formation of pyritic gold ores. Geology 47, 335–338.

Zhong, R., Brugger, J., Tomkins, A.G., Chen, Y., Li, W., 2015. Fate of gold and base metals during metamorphic devolatilization of a pelite. Geochim. Cosmochim. Acta 171, 338–352.

Zimmer, K., Zhang, Y.L., Lu, P., Chen, Y.Y., Zhang, G.R., Dalkilic, M., Zhu, C., 2016. SUPCRTBL: A revised and extended thermodynamic dataset and software package of SUPCRT92. Comput. Geosci. 90, 97–111.

Zotov, A.V., Shikina, N.D., Akinfiev, N.N., 2003. Thermodynamic properties of the Sb(III) hydroxide complex $Sb(OH)_3(aq)$ at hydrothermal conditions. Geochim. Cosmochim. Acta 67, 1821–1836.

Zotov, A.V., Kuzmin, N.N., Reukov, V.L., Tagirov, B.R., 2018. Stability of $AuCl_2^-$ from 25 to 1000 °C at pressures to 5000 bar and consequences for hydrothermal gold mobilization. Minerals 8, 286.

Figure captions

Figure 1. High-temperature part of the water phase diagram showing the domains of the different aqueous phases (liquid, vapor *sensu stricto*, and supercritical fluid) and three major types of geological fluids, labelled (A), (B) and (C) according to their *T*-*P*-density parameters and the degree of our knowledge of chemical speciation, solubility and thermodynamic properties as discussed in section 2.2. Gray lines indicate selected isochores of pure water (i.e. lines of equal density) labelled by the corresponding density values in g/cm^3. The domain boundaries are imaginary and roughly guided by the practical applicability of the HKF equation of state for most aqueous species for domain (A). The asymmetrical shape of domain (A) and the 0.4 and 0.7 isochores break is due to the Y-axis scale break at 500 bar.

Figure 2. Hard-soft classification of chemical elements in their geochemically common oxidation states.

Figure 3. General scheme of a computer code for thermodynamic modeling of fluid-rock-gas equilibria.

Figure 4. Example of thermodynamic modeling of fluid evolution in a generic context of porphyry-epithermal Cu-Au(-Mo) deposits (modified from Pokrovski et al. 2015). An initial magmatic fluid has the following typical composition as inferred from fluid inclusions and geochemical studies: 10 wt % NaCl equivalent, 2 wt % S, H_2S:SO_2 mole ratio = 1, 0.75 wt % Fe as $FeCl_2$, 0.30 wt % Cu as CuCl. The fluid, degassed from magma at 700 °C and 1.5 kbar, cools and decompresses in the liquid-phase domain in equilibrium with native Au and alkali aluminosilicate rocks (quartz-muscovite-potassic feldspar assemblage, pH of 5–6 at all temperatures), according to a common scenario of fluid evolution in a porphyry-epithermal setting (see Kouzmanov and Pokrovski, 2012 for more details). Curves show the concentrations of the indicated sulfur forms (in ppm S), Au total solubility (ΣAu, red curve), which is the sum of the major dihydrosulfide and subordinate monohydrosulfide and dichloride complexes (green curve) and the $Au(HS)S_3^-$ complex (pink curve), and total Fe and Cu solubility (ΣFe and ΣCu as dominantly chloride complexes; Table 2). Gray horizontal bars delimit the temperature range of the stability of the indicated minerals (Py = pyrite, Mag = magnetite, Bn = bornite, and Ccp = chalcopyrite) that precipitate on fluid cooling.

Figure 5. Example of thermodynamic modeling of fluid-rock interactions in the context of a gold sediment-hosted deposit (Shahuindo, northern Peru, described in Vallance et al., 2024). The following scenario is considered: an aqueous magmatic-derived S-Au-As-Fe bearing fluid of high-sulfidation type (sulfate-dominated, f_{O_2} > that of the hematite-magnetite buffer, HM) percolates through an hydrocarbon-bearing sandstone rock (represented by a C:H = 1 stoichiometry). The fluid is of moderate-salinity and acidic (7 wt % NaCl equivalent; 1 m NaCl + 0.1 m KCl + 0.05 HCl, pH ≈ 2.5), bearing 100 ppm of As and saturated with pyrite and metallic gold. The fluid reacts at 300 °C, 500 bar with a hydrocarbon-bearing shale at a mass fluid/rock ratio of 1:1 as a function of CH content in the rock. (a) Concentrations of total dissolved Au ($Au(HS)_2^- + Au(HS)S_3^-$), Fe ($FeCl_2 + FeCl_4^{2-}$), and As (as $As(OH)_3$) in the fluid and of As in arsenian pyrite (as $Fe(As,S)_2$ solid solution), as a function of the rock carbon content. Corresponding evolution of the fluid-phase concentrations (molality) of the sum of sulfide ($H_2S + HS^- + NaHS^0$), sulfate ($SO_4^{2-} + HSO_4^- + NaHSO_4^0 + NaSO_4^-$) and carbonate ($CO_2 + HCO_3^- + CO_3^{2-}$) types of species, $S_3^{\bullet-}$ ion, dissolved hydrogen and methane (b), and fluid pH and f_{O_2}, relative to the HM buffer

(c). Remarkably, organic matter promotes, rather than limits, gold transport by the fluid through organic carbon bearing sedimentary or metamorphic rock lithologies.

Figures: (here only for evaluation purposes; for production please use the vector-type high resolution figures supplied with the submission)

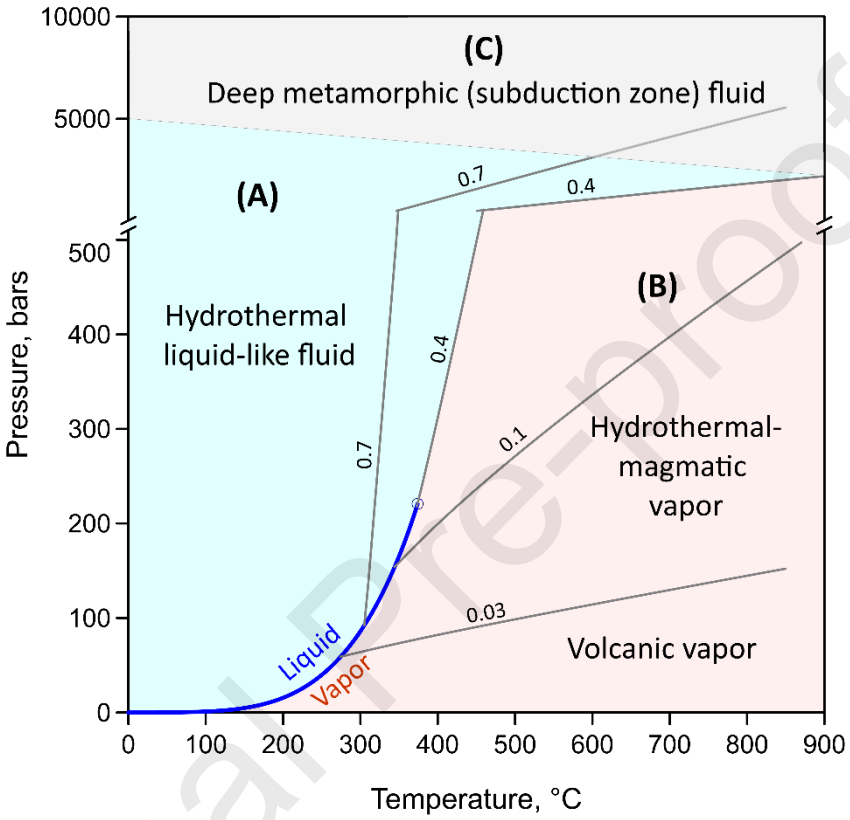

Figure 1. High-temperature part of the water phase diagram showing the domains of the different aqueous phases (liquid, vapor *sensu stricto*, and supercritical fluid) and three major types of geological fluids, labelled (A), (B) and (C) according to their *T*-*P*-density parameters and the degree of our knowledge of chemical speciation, solubility and thermodynamic properties as discussed in section 2.2. Gray lines indicate selected isochores of pure water (i.e. lines of equal density) labelled by the corresponding density values in g/cm^3. The domain boundaries are imaginary and roughly guided by the practical applicability of the HKF equation of state for most aqueous species for domain (A). The asymmetrical shape of domain (A) and the 0.4 and 0.7 isochores break is due to the Y-axis scale break at 500 bar.

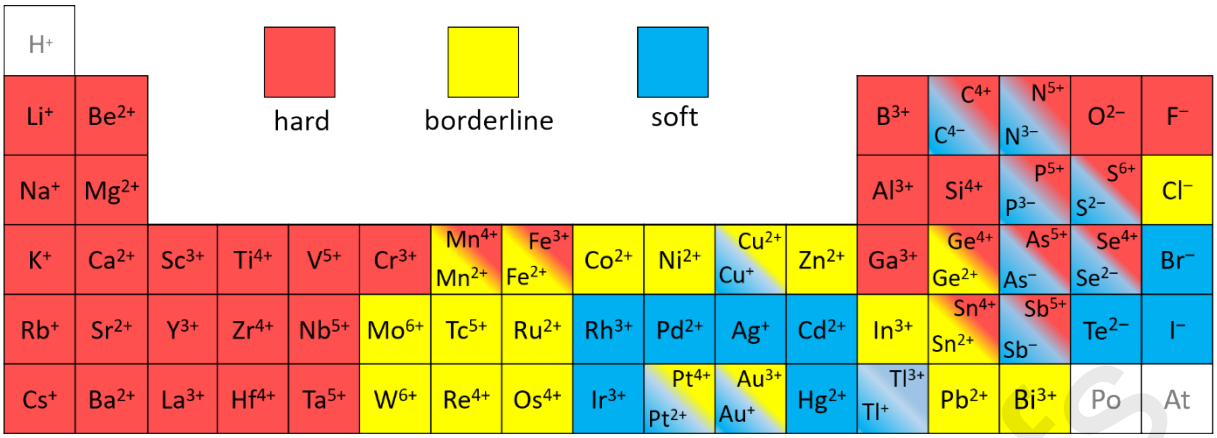

Figure 2. Hard-soft classification of chemical elements in their geochemically common oxidation states.

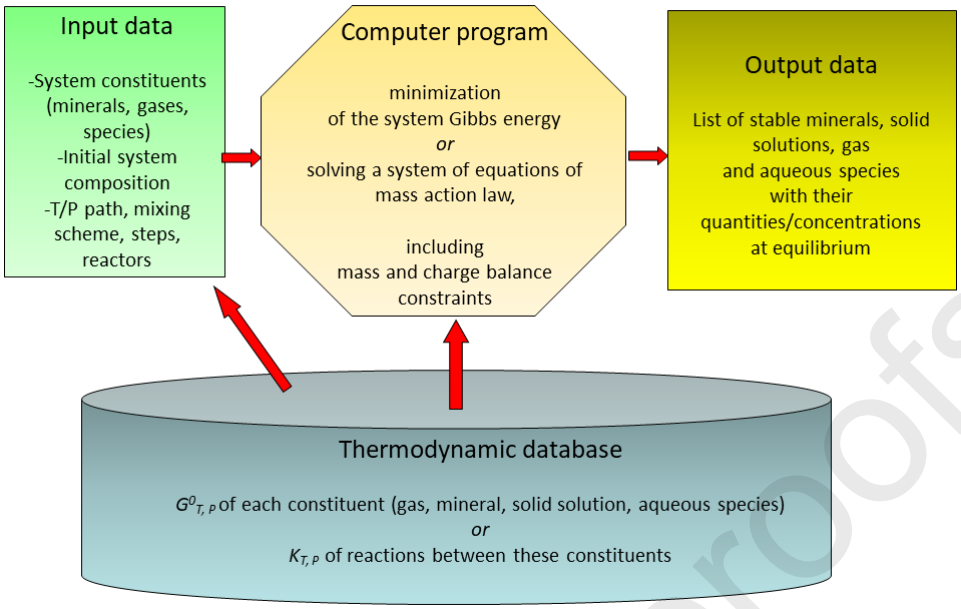

Figure 3. General scheme of a computer code for thermodynamic modeling of fluid-rock-gas equilibria.

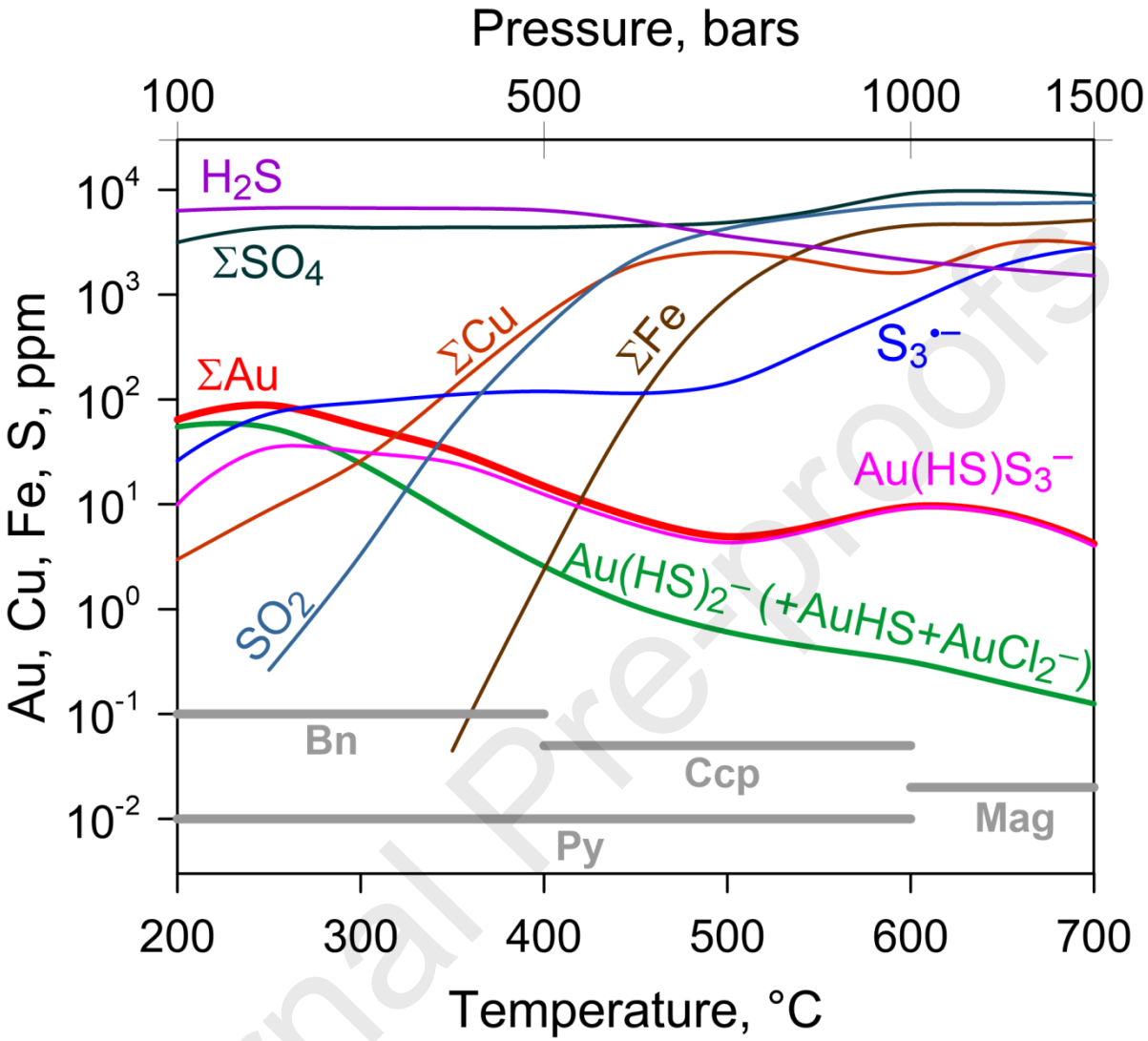

Figure 4. Example of thermodynamic modeling of fluid evolution in a generic context of porphyry-epithermal Cu-Au(-Mo) deposits (modified from Pokrovski et al. 2015). An initial magmatic fluid has the following typical composition as inferred from fluid inclusions and geochemical studies: 10 wt % NaCl equivalent, 2 wt % S, H_2S:SO_2 mole ratio = 1, 0.75 wt % Fe as $FeCl_2$, 0.30 wt % Cu as CuCl. The fluid, degassed from magma at 700 °C and 1.5 kbar, cools and decompresses in the liquid-phase domain in equilibrium with native Au and alkali aluminosilicate rocks (quartz-muscovite-potassic feldspar assemblage, pH of 5–6 at all temperatures), according to a common scenario of fluid evolution in a porphyry-epithermal setting (see Kouzmanov and Pokrovski, 2012 for more details). Curves show the concentrations of the indicated sulfur forms (in ppm S), Au total solubility (ΣAu, red curve), which is the sum of the major dihydrosulfide and subordinate monohydrosulfide and dichloride complexes (green curve) and the $Au(HS)S_3^-$ complex (pink curve), and total Fe and Cu solubility (ΣFe and ΣCu as dominantly chloride complexes; Table 2). Gray horizontal bars delimit the temperature range of the stability of the indicated minerals (Py = pyrite, Mag = magnetite, Bn = bornite, and Ccp = chalcopyrite) that precipitate on fluid cooling.

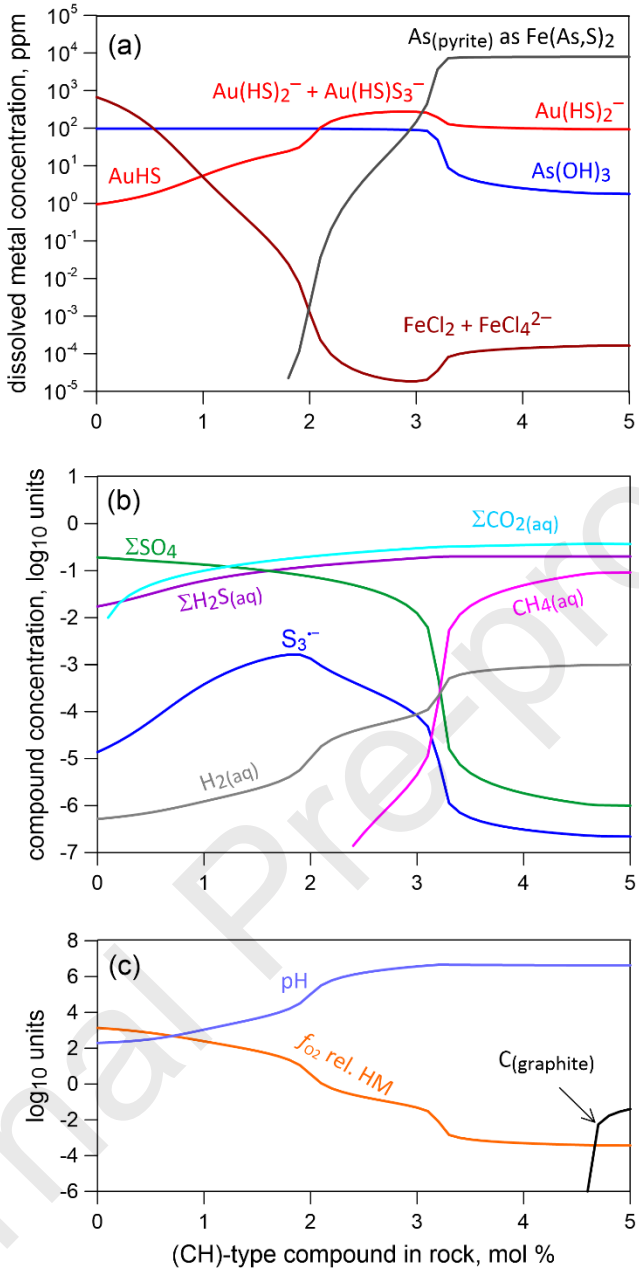

Figure 5. Example of thermodynamic modeling of fluid-rock interactions in the context of a gold sediment-hosted deposit (Shahuindo, northern Peru, described in Vallance et al., 2024). The following scenario is considered: an aqueous magmatic-derived S-Au-As-Fe bearing fluid of high-sulfidation type (sulfate-dominated, f_{O_2} > that of the hematite-magnetite buffer, HM) percolates through an hydrocarbon-bearing sandstone rock (represented by a C:H = 1 stoichiometry). The fluid is of moderate-salinity and acidic (7 wt % NaCl equivalent; 1 m NaCl + 0.1 m KCl + 0.05 HCl, pH ≈ 2.5), bearing 100 ppm of As and saturated with pyrite and metallic gold. The fluid reacts at 300 °C, 500 bar with a hydrocarbon-bearing shale at a mass fluid/rock ratio of 1:1 as a function of CH content in the rock. (a) Concentrations of total dissolved Au ($Au(HS)_2^-$ + $Au(HS)S_3^-$), Fe ($FeCl_2$ + $FeCl_4^{2-}$), and As (as $As(OH)_3$) in the fluid and of As in arsenian pyrite (as $Fe(As,S)_2$ solid solution), as a function of the rock carbon content. Corresponding evolution of the fluid-phase concentrations (molality) of the sum of sulfide (H_2S + HS^- + $NaHS^0$), sulfate (SO_4^{2-} + HSO_4^- + $NaHSO_4^0$ + $NaSO_4^-$) and carbonate (CO_2 + HCO_3^- + CO_3^{2-}) types of species, $S_3^{\bullet-}$ ion, dissolved hydrogen and methane (b), and fluid pH and f_{O_2}, relative to the HM buffer

(c). Remarkably, organic matter promotes, rather than limits, gold transport by the fluid through organic carbon bearing sedimentary or metamorphic rock lithologies.

Tables

Table 1. Composition of hydrothermal fluids from typical examples of active sources and fluid inclusions from metal hydrothermal-magmatic deposits and comparison with the Clarke element concentrations (in ppm).

Element	Geothermal brine, Salton Sea, 300 °C, USA[1]	H_2O-CO_2 ore fluid, gold-bearing quartz vein, 270 °C, Italy[2]	Quartz-cassiterite fluid vein, Mole Granite, 550 °C, Australia[3]	Average element concentration in the upper continental crust[4]
Na	50400	17314	78000	24300
K	17500	863	37000	23200
Ca	28000	793	3200	25700
Cl	155000	21389	266000	370
F	15	401	–	557
Br	120	104	420	1.6
Fe	2290	18	60000	39200
Al	4	272	–	81500
Sr	400	53	30	320
Cu	8	4	900	28
Zn	540	2	5200	37
Pb	102	3	3300	17

As	12	96	480	5
Au	0.0005 [5]	0.05 [6]	1 [7]	0.0015
SiO_2	400	900	5400	666000
B	390	432	–	17
S	–	–	1000–10000	621
SO_4	5	996	–	–
H_2S	16	340	–	–
CO_2	110	94500	–	7300 [8]

[1] Muffler and White, 1969; [2] Yardley, et al. 1993; [3] Heinrich, et al. 1992; [4] Rudnick and Gao, 2014; [5] McKibben et al., 1990; [6] Rauchenstein-Martinek et al., 2014, average value of similar veins; [7] Kouzmanov and Pokrovski, 2012, average of porphyry-deposit fluids; [8] Wedepohl, 1995.

Table 2. Solubility-controlling aqueous species and solids phases of selected gangue and ore elements in saline aqueous fluids (T = 150–500 °C, P < 2 kbar, density > 0.4 g/cm^3) at conditions relevant to hydrothermal deposit formation.

Element	Solubility-controlling solid phases	Dominant species in aqueous fluid [1]	Prediction quality [2]	Key recent references [3]
As	arsenopyrite, arsenian pyrite	$As(OH)_3^0$	good	Perfetti et al., 2008; Xing et al., 2019; Pokrovski et al., 2022b
Sb	stibnite, Cu-Fe-Sn sulfosalts	$Sb(OH)_3^0$, $Sb(OH)_2Cl^0$	fair	Zotov et al., 2003; Pokrovski et al., 2006
Ge	GeS_2, GeO_2, sphalerite, quartz, phyllosilicates	$Ge(OH)_4^0$	fair	Pokrovski et al., 2005
Ga	GaOOH, Al-oxy-hydroxides, Al-silicates	$Ga(OH)_2^+$, $Ga(OH)_4^-$	fair	Bénézeth et al., 1997; Diakonov et al., 1997
Zn	sphalerite	$ZnCl_2^0$, $ZnCl_3^-$, $ZnCl_4^{2-}$	good	Sverjensky et al., 1997; Akinfiev and Tagirov, 2014
Cd	greenockite, sphalerite			
Pb	galena	$PbCl_2^0$, $PbCl_3^-$, $PbCl_4^{2-}$	fair	Sverjensky et al., 1997
Fe	pyrite, magnetite, hematite, pyrrhotite	$Fe^{II}Cl_2^0$, $Fe^{II}Cl_4^{2-}$ $Fe^{III}Cl_n^{3-n}$	fair	Sverjensky et al., 1997; Testemale et al., 2009; Saunier et al., 2011; Gammons and Allin, 2022
Cu	chalcopyrite, bornite, enargite	$CuCl_2^-$, $Cu(HS)_2^-$	good	Akinfiev and Zotov, 2001; Liu and McPhail, 2005; Trofimov et al., 2023
Ag	argentite, sulfosalts	$AgCl_2^-$	good	Pokrovski et al., 2013b

Au	native gold; bound Au in pyrite and arsenopyrite	$Au(HS)_2^-$, $Au(HS)S_3^-$, $AuCl_2^-$	good	Pokrovski et al., 2014, 2015, 2021a, Zotov et al., 2018
Mo	molybdenite	$HMoO_4^-$, MoO_4^{2-}, MoS_4^{2-} *oxysulfides, oxychlorides, polysulfides*	poor	Dadze et al., 2018; Liu et al., 2020
Pt, Pd	cooperite, braggite, sperrylite, PGE substituted in pyrite, pyrrhotite, chalcopyrite	$Pt(HS)_2^0$, $Pt(HS)_4^{2-}$, $PtCl_4^{2-}$, $Pt(HS)_2(S_3)_2^{2-}$, $Pd(HS)_4^{2-}$, $PdCl_4^{2-}$	poor	Bazarkina et al., 2014; Kokh et al., 2017; Tagirov et al., 2019; Filimonova et al., 2021; Pokrovski et al., 2021b; Laskar et al., 2022, 2025
Si	quartz, major silicates	$Si(OH)_4^0$	good	Sverjensky et al., 2014; Miron et al., 2016
Al	muscovite, boehmite, corundum, feldspar	$Al(OH)_3^0$, $Al(OH)_4^-$, $(Na/K)Al(OH)_4^0$, $AlOSi(OH)_3^{2+}$, $Al(OH)_3OSi(OH)_3^-$	good	Salvi et al., 1998; Tagirov and Schott, 2001; Sverjensky et al., 2014; Miron et al., 2016
REE	monazite, bastnäsite, fluocerite	$REECl^{2+}$, $REECl_2^+$, $REE(SO_4)_2^-$	fair	Migdisov et al., 2016
S	pyrite, pyrrhotite, barite, gypsum, alunite	SO_4^{2-}, HSO_4^-, $NaSO_4^-$, H_2S^0, HS^-, SO_2^0, $S_3^{\bullet-}$	fair	Shock et al., 1997, Akinfiev and Diamond, 2003; Pokrovski and Dubessy, 2015

[1] Species shown *in italic* are expected to be significant but yet have poorly constrained stoichiometry and stability.

[2] Qualitative estimate as a rough uncertainty in predicting the metal dissolved concentration in equilibrium with its solid phases as a function of *T*, *P*, pH and S_2 and O_2 fugacity, using the available published stability constants for the corresponding aqueous species from different studies: good = <1 log unit, fair >1 to 2 log units, poor >2–3 log units. This estimate also includes uncertainties related to the solid solutions and trace element speciation in the solubility-controlling solid phase.

[3] Major selected experimental or theoretical studies explicitly reporting thermodynamic data for aqueous complexes that can directly be used in thermochemical calculations (numerous previous references can be found therein).

Table 3. Comparison of Au concentrations in equilibrium with native gold metal calculated using the equilibrium constant of reaction (2a) for typical compositions of geothermal, epithermal and porphyry fluids (average salinity of 5.5 wt% NaCl equiv., or 1 m NaCl) and their comparison with natural geothermal or fluid inclusion data. Solute concentrations are expressed both in units of ppm (analytical) and molality (m, mol/kg H_2O) (thermodynamic).

Setting	**H_2S, ppm**	**H_2S, m**	**H_2, ppm**	**H_2, m**	**pH**	**Log *K***	**Au, m calc.[3]**	**Au, ppm calc.**	**Au, ppm natural**
Deep geothermal waters and black smokers[1] 300 °C, 300 bar	50	0.0015	0.3	1.5×10^{-4}	5.0	9.8	7.1×10^{-9}	0.0014	$<10^{-4}$–0.02
Epithermal high-sulfidation Cu(-Au) deposits[2] 300 °C, 500 bar	5 000	0.15	1.0	5×10^{-4}	5.0	9.7	4.6×10^{-5}	9.0	0.1–20
Porphyry Cu-Au-Mo, some orogenic Au[2] 500°C, 1000 bar	10 000	0.29	100	0.05	5.0	11.7	2.6×10^{-7}	0.05	0.1–10

[1] Hannington et al., 2016; Simmons et al., 2016

[2] Kouzmanov and Pokrovski, 2012

[3] Activity coefficient of $Au(HS)_2^-$ is adopted as 0.4 and 0.3 at 300 °C (I = 0.6) and 500 °C (I = 0.2), respectively, according to equation (8).

Table 4. Selected computer codes and thermodynamic databases enabling thermodynamic equilibrium calculations in multicomponent mineral-fluid(-gas) systems.

Code/database	**Web address**
Supcrt92 database	http://geopig3.la.asu.edu:8080/GEOPIG/index.html
SupcrtBL database	https://models.earth.indiana.edu/applications_index.php
NIST-JANAF database	https://janaf.nist.gov/
Thermoddem database	https://thermoddem.brgm.fr/
MINES 2023 database	https://doi.org/10.58799/mines-tdb
CHNOSZ	https://chnosz.net/
HCh	http://www1.geol.msu.ru/deps/geochems/soft/index_e.html
EQ3/6	https://github.com/llnl/eq3_6
CHESS	http://chess.geosciences.mines-paristech.fr/
Geochemists Workbench (GBW)	https://www.gwb.com/index.php
PHREEQC	https://www.usgs.gov/software/phreeqc-version-3/
Visual MINTEQ	https://vminteq.lwr.kth.se/
GEM-Selektor	http://gems.web.psi.ch/
Perple_X	http://www.perplex.ethz.ch/